EURAS
JOURNAL
of Engineering and Applied Sciences

EURAS JOURNAL OF ENGINEERING AND APPLIED SCIENCES

Volume 3 Issue 2 August 2023

EURAS JOURNAL OF ENGINEERING AND APPLIED SCIENCES

Editorial Board

Scientific Advisory Board

Contents

DOI Numbers

From The Editor

Euras Journal of Engineering and Applied Sciences (EJEAS), is a peer-reviewed academic journal, establishing a solid platform for all academicians, consultants, researchers, and those who have a strong interest in global current issues and trends in engineering and applied sciences. Euras Journal of Engineering and Applied Sciences is based on engineering and applied sciences; artificial intelligence, cybersecurity, environmental sciences, food and food safety, biotechnology, material science and composites, nanotechnology, energy technologies, electronics, robotics, thermal sciences, earthquakes – structures – foundation and earth sciences studies. Subject areas could be as narrow as a specific phenomenon or device or as broad as a system.

EJEAS was established with the intention of promoting scholarly communication all over the world in a more effective manner. Our aim is to establish a publication that will be abstracted and indexed in the Engineering Index (EI) and Science Citation Index (SCI) in the near future. The journal has a short processing period to encourage young scientists.

Prof. Dr. Hasan HEPERKAN
Editor

The Impact of Cognitive Biases on User Decision Making in Human-Computer Interaction: A Review of the Literature

Irmak Saygı[1], Y. Birol Saygı[2]

[1]MSc Psychologist and Neuroscientist, London, UK ,irmaksaygi@gmail.com;
ORCID: 0000-0002-8051-7987

[2]Department of Mechanical Engineering, Istanbul, Turkey, leblebicioglu.emre@gmail.com;

ORCID: 0000-0001-9974-3645

ABSTRACT

Human-Computer Interaction (HCI) is an interdisciplinary subject that studies the interaction between humans and computers. Cognitive biases are systematic errors in human reasoning and decision-making which is suggested to affect interactions of users with computers. This study aims to contribute to the bridge the gap in the literature by addressing the impact of cognitive biases on user decision-making in HCI and discuss the practical applications of the currently literature. Accordingly, a literature search was conducted using electronic academic databases. The reviewed papers were mainly focused to articles published in the last 10 years (2003-2013) to ensure the relevance of the literature to current research questions. Our research revealed four factors (the quantity of available and accessible information, the lack of meaning associated with the information, the need for quick action, and what information is remembered or recalled) that can trigger cognitive biases and how they can further impact decision making processes of users through common biases. An explored two common strategies (user research and digital nudging) for designing interfaces that minimize negative effects of cognitive reductions. Our findings provide a valuable contribution to the literature and aimed to lead a better user experiences and greater user satisfaction with technology.

Keywords: *Human-Computer Interaction, Cognitive Biases, User Experience, User Experience Research*

1. INTRODUCTION

Often referred to as HCI, Human-Computer Interaction is an interdisciplinary subject that studies the interaction between humans and technological artifacts, and their designs. [1]. HCI encompasses a wide range of subjects, including engineering, behavioural sciences, and design [2]. HCI aims to support human activities is intuitive, efficient, and effective [3]. It can also contribute to the development of new technologies and applications that address important societal challenges, such as healthcare, education, and environmental sciences [4].

As computers and other digital devices become increasingly ubiquitous in our daily lives, HCI plays a critical role in shaping the way people interact with technology through such user platforms as online shopping, social media, healthcare services etc. [5]. Accordingly, these platforms use the user interfaces (UI) serve as the primary means of interaction and communication between humans and computers on a technological device. An effective interface design can help to ensure that technology is user-friendly and accessible to a wide range of people, including those with disabilities or limited technical knowledge and can lead to improved productivity, better decision making, and increased user satisfaction [6] [7]

There are several ways how the research in the field of HCI contributes these outcomes: Such as developing methodologies that enable user experience (UX) designers and UX researchers to prototype and test machine interfaces even prior to their deployment to end-users or creating techniques that can produce "engineering models of human performance" which can predict human performance on computer tasks before they are carried out. John and Kieras [8] provide a detailed overview and comparison of these tools, which are similar to models used in the physical sciences [9]. As these and many other examples suggest studying and understanding human factors (cognitive processes and behaviours) and their effects on humans' interactions with the computers are significant parts of the HCI research for creating technology that is user-centred and able to meet the needs of users in diverse contexts [10].

Cognitive biases are one of the key human factors studied by HCI researchers which is initially defined by Tversky and Kahneman in 1974 as inherent flaws or systematic errors in human reasoning and decision-making [11] [12]. There are several explanations why cognitive biases occur however, the vast amount of literature tends to explain this phenomenon with dual-processing theories which suggest that mental processes can be divided into two categories as controlled and automatic processes [13]. Accordingly, controlled processes are initiated intentionally, require considerable cognitive resource, and operate within

conscious awareness. In contrast, automatic processes are initiated unconsciously, require minimal cognitive resources, and operate quickly. In his well-known book Thinking, Fast and Slow [14], Kahneman described these processes as System 1 (referring to automatic processes) and System 2 (controlled processes) and suggested System 1 can led to faster decisions, but it can be error-prone due to biases and heuristics. System 2 tends to be more reliable, but it requires more cognitive effort and slows down decision-making [15].
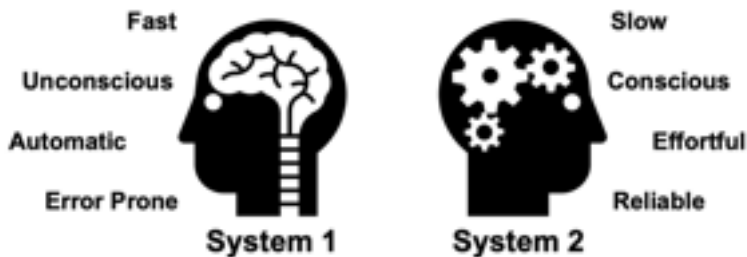
Figure 1. System 1 and System 2 demonstration based on Thinking, Fast and Slow [14]

Thereby, Cognitive biases can simplify decision-making by reducing the amount of information and uncertainty that needs to be processed [16]. Therefore, it is imported to note that although cognitive biases are typically assumed to have a negative impact, they can have positive impacts as well. On the other hand, the intensity of the biases can differ in people due to the combination of evolutionary, societal, and environmental factors, as well as individual differences in cognitive processing [17].

Overall, while there is no consensus, the number of reported biases currently exceeds 180, with different categorizations of these biases proposed in the literature [18]. Moreover, cognitive biases are often unconscious and can be difficult to detect, making them a significant challenge in many fields, including HCI [19]. The presence of the bias can result with the adoption of the irrational beliefs and early inferences without following any objectivity [20]. As the concern of this paper, these biases not only affect the judgement of the users but can further dictate their decisions which is undesirable in a user-centred computer interface design [21]. Accordingly, this study aims to contribute to the bridge the gap in the literature by providing a review of the overall themes and trends in the literature regarding to the nature of the interaction between the two concepts. Accordingly, our research questions are: (22) How cognitive biases impact user decision making in HCI? (2) What are the practical applications suggested in literature for reducing the bias in HCI?

2. METHODOLOGY

A systematic literature search was conducted using electronic databases such as Google Scholar, ACM Digital Library, Frontiers, and Elsevier. The reviewed papers were mainly focused to articles published in the last 10 years (2003-2013) to ensure the relevance of the literature to current research questions. The following search terms will be used: "cognitive bias," "decision making," "human-computer interaction," "HCI," and "user interface." Articles will be screened based on their relevance to the research questions, with a focus on studies that address the impact of cognitive biases on user decision-making in HCI, identify common biases that users face while interacting with computers, and discuss the practical applications of the current literature. Nevertheless, studies were included in this review if they meet the following criteria: (a) published in English language, (b) conducted empirical research related to cognitive biases and their impact on users' decision making in HCI, (c) published in peer-reviewed journals, conference proceedings or books. Studies were excluded if they do not meet the inclusion criteria or if they are duplicate studies. The quality of the studies will be assessed using established quality assessment tools such as statistical reliability parameters. There were no ethical issues are anticipated for this literature review.

3. EMPRICAL REVIEW

3.1. How Cognitive Biases Impact User Decision Making in HCI?

Our research identified various factors can trigger cognitive biases and further impact decision making processes of users. These factors are: (23) the quantity of available and accessible information, (24) the lack of meaning associated with the information, (25) the need for quick action, and (26) what information is remembered or recalled. Based on the systematic review of Azzopardi [27] these factors as overall categories of biases can initially associated with search behaviour of users in various platforms including web-based user interface design. We conducted current review through this perspective for narrowing the scope of the study.

3.1.1. Quantity of Available Information

Social psychology theories suggest that various cognitive biases can affect human decision making based on their engagement and elaboration

with the available content [28]. Accordingly, information overload which is a situation where a person is presented with an excessive amount of information while attempting to perform a task or make a decision (IDF) which is commonly observed in various online environments [29]. In contrast, lack of information might lead users to make uninformed early interferences regarding the information. On both situations, it is found that individuals tend to make decisions based on emotions, simple rules, or social cues due to the reduced motivation and reduced use many cognitive resources which induce cognitive biases [30]. Therefore, the amount of available and accessible information in a user interface of a platform such as a social media channel can lead users to notice paying attention and even favouring information that is already primed in memory or repeated overly in the interface [31].

Our research revealed the confirmation bias as the most common theme under this subject (e.g., [32] [33] [34] [35] [36] [37]). Confirmation bias refers to the tendency to seek, interpret, and remember information in a way that confirms one's pre-existing beliefs or hypotheses while ignoring or dismissing information that contradicts them (Nickerson, 1998). Accordingly, there are several situations that confirmation bias has studied in the HCI context. For example, Suzuki and Yamamoto [38] observed confirmation bias in the context of web search behaviour. They exemplified the process by referring to an imaginary health-conscious user (X), who watches a TV program claiming that genetically modified food Y is harmful to health. Subsequently, when X searches the web to gather more information about food Y's safety, X suggested more likely to focus on information that confirms his belief that food Y is harmful. This unconscious tendency to seek out information that supports pre-existing beliefs is known as confirmation bias. Even if the information that X finds is inaccurate or low-quality, they may still give it preference over information that contradicts their existing beliefs. Accordingly, their study with overall 300 participant showed that participants with poor literacy and negative prior beliefs about the searched topic spend significantly less time going through the web search results compared the ones with positive and neutral beliefs. Supporting this, the study by Pothirattanachaikul et al. [39] found that participants spent more time in searching through documents when they were presented with belief inconsistent documents.

3.1.2. Lack of Meaning Associated with the Information

Experiencing certain events without lack of attached meaning or explanation may lead false attributions and errors in decision-making such as stereotyping or generalising a situation based on prior knowledge or beliefs causing positive inferences to familiar things [2]. Our research found that this commonly leads to the bias which is known with the names of bandwagon effect, group thinking and herd behaviour [2]. The bias occurs when individuals tend to adopt a particular behaviour, style, or attitude because they observe others doing so [19]. The greater the number of people adopting the trend, the more likely it is for others to follow suit [4]. This effect has found its reflection in decision-making process through various computer interfaces that allows content creation, product reviews, peer recommendations and question-answering (Q&A) [9]. Accordingly, Kelly et al. [15] asked 128 participants to use a computer-based search engine to find information about four topics while their interactions with the engine were recorded. During the task, search engine provided query suggestions that varied in popularity and quality. Although researchers found both popularity and quality of query suggestions significantly affected the participants' selection of queries, popularity had a stronger effect on the participants compared to quality of the queries. The findings suggest that users may be biased due to the bandwagon effect, even at the expense of quality and accuracy of the information. Another study by Lewandowsky et al. [19] with over 1,000 social media users showed that users tend to share articles that have already been widely shared by others, which is another indication of bandwagon effect in HCI context.

3.1.3. Need for Quick Action

Time pressure in decision making can lead to biased thoughts such as preferring simple options over complex ones or/and prioritizing preservation of autonomy and group status as well as avoiding irreversible decisions to prevent any mistake [2]. Accordingly, combination of time pressure and user interface design may trigger decoy effect in participants which might lead faulty decisions. The decoy effect is a cognitive bias where an option becomes more attractive when it is presented alongside an unattractive option (decoy). In the study conducted by Tietz et al. [37], when 96 participants were presented with the choice of receiving an e-book for a $10 pledge (Competitor) or both an e-book and a hardcover book for a $20 (Target) pledge, most of them chose the former (69%). However,

when a decoy option was introduced that offered only the hardcover book for $20, most of them chose to pledge $20 to receive both books (68%). The decoy option nudged backers towards the more expensive option, resulting in more pledges. Table 1 presents an overview of the choice sets of the two scenarios.

Table 1: Choice sets for the book scenario [37]

Option	Baseline Condition	Decoy Condition
Option A	PAY $10 – GET an eBook	PAY $10 – GET an eBook
Option B (Decoy)		PAY $20 – GET a hardcover book
Option C	PAY $20 – GET an eBook and a hardcover book	PAY $20 – GET an eBook and a hardcover book

Further studies by Wu and Cosguner [40] and Sherlin et al. [41] also reported decoy effect on real online shopping settings which suggest the possible use of decoy pricing to increase sales and revenue by strategically pricing their products in a way that influences user behaviour. However, some researcher caution that the use of decoy pricing may not be suitable for all product categories and may have ethical implications that should be carefully considered since users may not be aware that their decision is being influenced by the presence of the decoy option. [42].

3.1.4. What to Remember or Recall

To cope with the need to retain information selectively from the available content, people tend to select and store certain elements of events and lists. They may also edit and reinforce memories based on how they were experienced [43]. Nevertheless, we found that most bias which were considered under this group showed challenging results in the scope of HCI. For instance, priming effect which is commonly suggested to influence over the attitudes and experience toward technology [45] [46] [47]. For example, the study by Ferreri et al. [48] found that the according to their primed expectations (negative, positive, or neutral) toward the technology in online scavenger hunt, participants (N=42) showed significantly different attitudes in their responses to failures in digital technology.

In contrast, further study by Hawes and Arya [49] with 51 participants conducted to understand whether virtual environments can be created in a way that boosts participation and proficiency in various cognitive tasks. Accordingly, participants were assigned three different conditions (virtual reality learning spaces) as animation studio (primed condition), theatre with animation artifacts (primed condition) and theatre without animation artifacts (no-primed condition) while receiving a seminar with same educational content. Although results found an increase in general user-experience as well as academic performance, no significant difference found between the groups.

3.2. What are the Practical Applications Suggested in Literature for Reducing the Cognitive Biases in HCI?

Reducing the negative effects of cognitive biases in user experience is another important topic in HCI since they can lead errors, decrease performance, and reduce user satisfaction [50]. In addition to its general impact, it is also suggested that HCI systems can be designed more inclusive, as certain biases may disproportionately affect certain groups [51] [52]. However, Adams et al. [53] discovered that the majority (94%) of behavior change technologies featured in HCI publications target the reflective mind (System 2), which is the deliberate and conscious decision-making process, rather than the fast and automatic mental processes (System 1) that govern an estimated 95% of our daily choices which suggests the technology is produced information-centric rather than user-centric [3]. In other words, users are left frail toward cognitive biases in their interactions with computers which possibly affect their decision-making. Nevertheless, there are several practical applications suggested in the literature for reducing cognitive biases in HCI including (1) user research and (2) digital nudging.

3.2.1. User Experience Research

User experience research or user research (UXR) refers to the process of under-standing the needs, behaviours, motivations, and pain points of users through various research methods such as user interviews, surveys, and usability testing [54]. User research is an effective method to reduce cognitive biases in HCI. Study by Olson and Olson [55] suggested that user research helps in reducing assumptions and biases by providing insight into users' mental models and cognitive process-es. This information can be used to design. user interfaces that are more intuitive and aligned with user needs [56]. As noted by Preece et al. [57], user research helps designers to "develop empathy with users and design for their needs, rather than designer or business needs."

Table 2: Definitions of common UXR methods [58] [59]

Research Methods	Definition
User Interview	A one-on-one conversation with a user to gather information about their thoughts, feelings, and behaviours
Surveys	A questionnaire designed to gather data from a large group of users in a structured way.
Usability Testing	An evaluation of a product or prototype with real users to identify usability issues and areas for improvement.
Contextual Inquiry	An in-person observation of a user in their natural environment to understand how they interact with a product or service.
Heuristic Evaluation	An expert evaluation of a product or prototype based on a set of usability principles or heuristics.

User research can be classified into two categories: exploratory research and evaluative research. Exploratory research aims to understand the users' needs, preferences, and behaviours, while evaluative research evaluates the usability and effectiveness of a product or service [60]. User research can help to evaluate the effectiveness of design solutions in reducing cognitive biases in both stages. For instance, before coming up with any design solution, detailed interviews with users may reveal established cognitive biases of users like stereotyping, whereas researchers may conduct usability testing to observe how users interact with the further design solution and identify potential sources of cognitive bias or other usability issues in testing process. This gives opportunity to stakeholders, engineers, and designers to come up possible solutions that reduce observed biases in final product.

3.2.2.Digital Nudging
Nudging is a technique that involves subtly influencing people's behaviour without taking away their freedom of choice [61]. Nudging can be used to

encourage people to make healthier choices or engage in environmentally friendly behavior [62]. For example, supermarkets places certain items like snacks, gums, or drinks next to the checkout services to nudge their customers into making unplanned purchases. Alternatively, nudges are not only used in physical environments. Accordingly, digital nudging refers to the use of user interface design and other digital tools to influence the behaviour of users in a predictable and positive way [63].

There is a considerable number of studies regarding the effect of digital nudges where a systematic review by Caraban et al. [64] identified 23 distinct mechanisms of nudging that affect user behaviour in various levels through analysing 71 articles from 13 prominent HCI venues. For example, they referred to the NewsCube which is an innovative online news platform that designed to address media bias including confirmation bias. The platform gathers articles from diverse sources, removes irrelevant information, and clusters the content into balanced sections, while highlighting unread sections to nudge users to explore all viewpoints [65]. Another example for digital nudging comes from Lee et al. [66] who utilized the decoy effect to encourage healthier snack choices on a website where users could order snacks. They placed a picture of a large and visually appealing Fuji apple next to a small and unappealing apple to increase the likelihood of users choosing the fruit over a cookie.

Overall, it has been showed that digital nudging has been applied in various contexts such as e-commerce, digital platforms for education, health, and wellness to promote positive behaviour change, improve decision-making, and increase engagement with digital platforms [67] [68]. However, ethical concerns around the use of digital nudging, particularly around issues of privacy, autonomy, and informed consent should be considered in practical use as well as being studied as a significant research topic in HCI.

4. CONCLUSION

Overall, this study aimed to examine the impact of cognitive biases on user decision-making in Human-Computer Interaction (HCI) and explore practical applications of the current literature. Our research identified factors such as the quantity of available information, the lack of meaning associated with the information, the need for quick action, and what information is remembered or recalled, which can trigger cognitive biases and impact

user decision-making. Furthermore, we discussed two common strategies, user research and digital nudging, which can minimize negative effects of cognitive biases in interface design. Our findings not only contribute to the literature but also have practical implications, such as improving user experiences, productivity, and satisfaction with technology.

The limitations of this study include the reliance on academic databases, which may not capture all relevant literature, and the potential for publication bias, as studies with significant findings may be more likely to be published. Additionally, the review will be limited to articles published in English and may not capture non-English literature on the topic. Nevertheless, our literature review highlights the need for designers and developers to be aware of the impact of cognitive biases on users' decision making in HCI. By designing interfaces that consider the influence of cognitive biases, we can create systems that are more user-friendly and effective. Further research is needed to explore the effectiveness of different design strategies in mitigating the impact of cognitive biases on users' decision making in HCI.

REFERENCES

[1] Adams, A. T., Costa, J., Jung, M. F., & Choudhury, T. "Mindless computing: designing technologies to subtly influence behavior,". In Proceedings of the 2015 ACM International Joint Conference on Pervasive and Ubiquitous Computing, pp.719–730, 2015.

[2] Azzopardi, L., "Cognitive Biases in Search: A review and reflection of cognitive biases in Information Retrieval," In Proceedings of the 2021 ACM SIGIR Conference on Human Information Interaction and Retrieval (CHIIR '21), 2021.

[3] Caraban, A., Karapanos, E., Gonçalves, D., & Munson, S. A., "23 ways to nudge: A review of technology-mediated nudging in human-computer interaction," ACM Computing Surveys (CSUR), vol. 52(4), pp.1-36, 2019.

[4] Cherry, K., "What is the Bandwagon Effect?" Verywell Mind, August 29, 2021, Retrieved April 25, 2023, from https://www.verywellmind.com/what-is-the-bandwagon-effect-2795895

[5] Dix, A., Finlay, J., Abowd, G., & Beale, R., Human-Computer Interaction,-

Prentice Hall, 2004

[6]   Dumas, J. S., & Redish, J. C, "A practical guide to usability testing," Intellect Books, 1999.

[7]   Ferreri, N., & Mayhorn, C. B., "Examining frustration and performance when priming user expectations and providing a technology malfunction," Proceedings of the Human Factors and Ergonomics Society Annual Meeting, vol. 64(1), pp:1846–1850, 2020.

[8]   Gopal, D. P., Chetty, U., O'Donnell, P., Gajria, C., & Blackadder-Weinstein, J., "Implicit bias in healthcare: clinical practice, research and decision making," Future healthcare journal, vol. 8(1), pp.40–48., 2021.

[9]   Hao, H., Bedeley, R. T., & Torupallab, G., "Cognitive Biases in Online Opinion Platforms: A Review and Mapping," Available at SSRN: https://ssrn.com/abstract=4059282

[10]   Harrison, S., Tatar, D., & Sengers, P., "The three paradigms of HCI," In Proceedings of the 28th international conference on Human factors in computing systems, pp. 1-18, 2010.

[11]   Haselton, M. G., & Nettle, D., "The paranoid optimist: an integrative evolutionary model of cognitive biases," Personality and social psychology review: an official journal of the Society for Personality and Social Psychology, vol. 10(1), pp.47–66, 2006.

[12]   Hawes, D., & Arya, A.. "A VR-based Priming Framework and Technology Implementation to Improve Learning Mindsets and Academic Performance in Post-Secondary Students." arXiv preprint arXiv:2303.11547, 2023.

[13]   John, B. E. & Kieras, D. E., "The GOMS family of analysis techniques: Tools for design and evaluation," School of Computer Science Technical Report CMU-CS-94-181, Human-Computer Interaction Institute Technical Report CMU-HCII-94-106. Pittsburgh, PA: Carnegie Mellon University, 1994.

[14]   Kahneman, Daniel. Thinking, Fast and Slow. Farrar, Straus and Giroux, 2011.

[15]   Kelly, D., Cushing, A., Dostert, M., Niu, X., & Gyllstrom, K., "Effects

of popularity and quality on the usage of query suggestions during information search," In Proceedings of the SIGCHI Conference on Human Factors in Computing Systems (CHI '10), pp. 45-54, 2010.

[16]   Koester, T., Kierkegaard, H., Jakobsen, J., Toft, N., & Bang, C., "How to Program Positive Medical Device User Experience Using Narratives, Storytelling and Priming." Proceedings of the International Symposium on Human Factors and Ergonomics in Health Care, vol. 5, pp.89-93, 2016.

[17]   Lazar, J., Feng, J. H., & Hochheiser, H., Research Methods in Human-Computer Interaction, Morgan Kaufmann Publishers, Massachusetts, 2017.

[18]   Lee, J., Lee, H., Kim, J., & Choi, Y., "Using the decoy effect to nudge healthier snack choices among adolescents," Journal of health communication, vol. 20(8), pp.964-971, 2015.

[19]   Lewandowsky, S., Ecker, U. K., Seifert, C. M., Schwarz, N., & Cook, J., "Misinformation and Its Correction: Continued Influence and Successful Debiasing," Psychological science in the public interest: a journal of the American Psychological Society, vol. 13(3), pp. 106–131, 2012.

[20]   Nielsen, J., Usability engineering. Morgan Kaufmann Publishers, Massachusetts, 1994.

[21]   Norman, D. A., & Draper, S. W., User centered system design: New perspectives on human-computer interaction, L. Erlbaum Associates, New York, 1986.

[22]   Novin, A. & Meyers, E.M., "Four Biases in Interface Design Interactions," Design, User Experience, and Usability: Theory, Methodology, and Management, Lecture Notes in Computer Science, Springer, vol. 10288, 2017.

[23]   Olson, G. M., & Olson, J. S., "Human-computer interaction: psychological aspects of the human use of computing," Annual Review of Psychology, vol. 54, pp. 491-516, 2003.

[24]   Park, H., Lim, Y., & Kim, M., "NewsCube: Delivering multiple aspects of news to mitigate media bias," International Journal of Human-Computer Studies, vol. 71(6), pp.606-620, 2013.

[25]   Pothirattanachaikul, S., Yamamoto, T., Yamamoto, Y., & Yoshikawa M., "Analyzing the Effects of Document's Opinion and Credibility on Search Behaviors and Belief Dynamics," In Proceedings of the 28th ACM International Conference on Information and Knowledge Management (CIKM '19), pp. 1653–1662, 2019.

[26]   Preece, J., Rogers, Y., & Sharp, H., "Interaction design: beyond human-computer interaction," John Wiley & Sons, 2015.

[27]   Pronin, E., "Perception and misperception of bias in human judgment," Trends in Cognitive Sciences, vol. 11(1), pp.37-44, 2007.

[28]   Rogers, Y., "Interaction design gone wild: striving for wild theory," Interactions. Vol. 18, 4, pp.58–62, 2011.

[29]   Rohrer, C., "Which UX Research Methods?" Nielsen Norman Group, July 17, 2022, Retrieved April 30, 2023, from https://www.nngroup.com/articles/which-ux-research-methods/

[30]   Rubin, J., Handbook of Usability Testing: How to Plan, Design, and Conduct Effective Tests (2nd ed.). John Wiley & Sons, 2016.

[31]   Schneider, F. M., Weinmann, M., & vom Brocke, J., "Digital nudging: Guiding online user choices through interface design. Communications of the Association for Information Systems," vol. 44, pp.424-442, 2019.

[32]   Sherlin, I., Siswadhi, F., & Sarmigi, E., "Analysing the decoy effect on online product purchasing preference: An experimental study," Proceedings of the 6th Annual International Conference on Management Research (AICMaR 2019), pp. 125-130, 2019.

[33]   Shneiderman, B., & Plaisant, C., Designing the User Interface: Strategies for Effective Human-Computer Interaction, Pearson Addison-Wesley, Boston, 2009.

[34]   Stanovich, K. E., & West, R. F., "On the relative independence of thinking biases and cognitive ability," Journal of Personality and Social Psychology, vol. 94(4), pp.672–695, 2008.

[35]   Suzuki, M. & Yamamoto, Y., "Analysis of Relationship between Confir-

mation Bias and Web Search Behavior," In Proceedings of the 22nd International Conference on Information Integration and Web-based Applications & Services (iiWAS '20), pp.184–191, 2021.

[36]   Thaler, R.H., & Sunstein, C.R., "Nudge: Improving Decisions About Health, Wealth, and Happiness," Yale University Press, New Haven, CT, and London, U.K., 2008.

[37]   Tietz, M., Simons, A., Weinmann, M., & Brocke, vom, J. "The decoy effect in reward-based crowdfunding: Preliminary results from an online experiment," In Proceedings of the International Conference on Information Systems (Dublin, Ireland, Dec. 11–14). Association for Information Systems, Atlanta, GA, pp. 1–11, 2006.

[38]   Tversky, A., & Kahneman, D., "Judgment under uncertainty: Heuristics and biases," Science vol. 185, pp.1124–1131, 1974.

[39]   Venkatesh, V., Brown, S. A., & Bala, H., "Bridging the qualitative-quantitative divide: Guidelines for conducting mixed methods research in information systems," MIS Quarterly, vol. 36(1), pp.21-54, 2012.

[40]   Vera, A. H., "Understanding Users: The Knowledge-Level of Analysis,"Human Factors in Information Technology, North-Holland, vol. 13, pp.89-103, 1999.

[41]   Wu, C., & Cosguner, K, "Profiting from the Decoy Effect: A Case Study of an Online Diamond Retailer" Marketing Science, vol. 39:5, pp.974-995, 2020.

[42]   Wu, L., Liu, P., Chen X., Hu, W., Fan, X., & Chen Y., "Decoy effect in food appearance, traceability, and price: Case of consumer preference for pork hindquarters," Journal of Behavioral and Experimental Economics, vol. 87, 2020.

[43]   Yamamoto, Y. & Yamamoto, t., "Query Priming for Promoting Critical Thinking in Web Search," In Proceedings of the 2018 Conference on Human Information Interaction & Retrieval (CHIIR '18), pp.12–21, 2018.

Diabetic Retinopathy Detection Using Meta Learning and Deep Learning Techniques

Muhammad Ammar Khan[1] , Ali Okatan[2]

[1]Department of AI & Data Science, Istanbul Aydin University, Istanbul,
mamarkhan@stu.aydin.edutr

[2]Prof. Dr. at Department of AI & Data Science, Istanbul Aydin University, Istanbul,
aliokatan@aydin.edu.tr ORCID: 0000-0002-8893-9711

ABSTRACT

ꙮIn the world of ocular health, diabetic retinopathy is a common condition that, if not recognized and treated promptly, can cause vision loss. In this study we present a meta learning stacking approach for the diagnosis and referral of ocular defects. Our approach demonstrates exceptional efficacy in detecting uncommon conditions by utilizing a combination of pre-trained convolutional neural networks (CNNs) and stacking meta-learning techniques. This novel approach improves the accuracy of results while significantly reducing the time required compared to conventional deep learning methods. The method demonstrates the promise of stacking meta learning in addressing data scarcity and improving early diagnosis of sight-threatening diseases by achieving an outstanding accuracy of 93%. Additionally, the solution beats problems brought on by a lack of readily available data which needs to be preprocessed. When compared to other deep learning models frequently used in ocular abnormality detection. These findings underscore the potential impact of our approach as an advanced computer-aided diagnosis tool for ocular anomalies, paving the way for significant advancements in the field. These valuable insights provide a solid foundation for future research, driving innovation and progress in computer-aided diagnosis tools for ocular health.ꙮ

Keywords: *Meta learning; Deep Learning; Retinopathy Detection; Diabetic*

Reinopathy

1. INTRODUCTION

Diabetic retinopathy (DR) is a prevalent and serious complication of Diabetes Mellitus, characterized by progressive vascular disruptions in the retina caused by chronic hyperglycemia [1]. It has become a significant global cause of visual impairment, impacting a staggering 93 million individuals worldwide and often leading to blindness among working-age adults. Timely detection and appropriate management of DR are crucial in preventing vision loss, making regular eye screening for diabetic patients essential. The manual diagnosis of DR through fundus examination by skilled ophthalmologists poses challenges in terms of expertise, time, and accessibility, particularly in densely populated or remote areas with limited access to specialized healthcare professionals.

To address these challenges, researchers have increasingly relied on artificial intelligence (AI) and deep learning (DL) methodologies to create computer-aided diagnosis systems for diabetic retinopathy (DR). DL models, empowered by deep neural networks, have shown promising capabilities in analyzing fundus images for automated DR detection, classification, and severity grading [2]. These models can accurately identify retinal lesions and assess the progression of DR, providing valuable insights for timely intervention and treatment. Moreover, DL-based models offer the potential to bridge the gap in access to specialized eye care, particularly in regions with a shortage of ophthalmologists. In this journal paper, we present an integrated review of meta-learning based approach for DR detection and classification. Our aim is to provide a comprehensive overview of the advancements, challenges, and future prospects in this rapidly evolving research area. Specifically, we will examine the technical implementations, dataset characteristics, preprocessing techniques, and model performance of published studies in the field. By analyzing the complete data analysis pipeline, including dataset selection, preprocessing, DL model development, and real-world implementation, we aim to offer valuable insights into the current state and potential of meta-learning in diabetic retinopathy diagnosis. By objectively analyzing the benefits and drawbacks of various DL models used to study diabetic retinopathy, we want to provide insight on their relative merits and clinical applicability. Additionally, we will discuss the ethical considerations and interpretability of DL models in addressing the challenges posed by DR diagnosis, emphasizing the importance of fairness,

transparency, and robustness in these AI-powered systems. By providing a comprehensive analysis of DL-based approaches for diabetic retinopathy, this journal paper aims to contribute to the advancement of meta-learning research in the field and support the development of accurate, efficient, and accessible diagnostic tools. Ultimately, our goal is to enhance the early detection and management of diabetic retinopathy, thereby reducing the burden of vision loss associated with this prevalent complication of diabetes.

2. RELATED WORK

Indeed, artificial intelligence technologies have greatly advanced the field of identifying diabetic eye disorders. Sarki et al., with its fine-tuned VGG16 model [3] and Nazir et al., The DenseNet-100 model along with a custom CenterNet model made significant progress by successfully using convolutional neural networks (CNNs) to analyze retinal pictures [4]. Their improved models and deep learning techniques significantly improved the detection and classification of glaucoma and diabetic eye disorders. Another important development in this area was a study that used meta-learning CNNs to identify diabetic retinopathy [5]. They suggested data resampling techniques for the selection of the training and validation set, then trained their CNNs using the chosen data. Additionally, they experimented with two ensemble learning strategies: meta-learner and unweighted average, and used straightforward data augmentation techniques to diversify the training data patterns. The meta-learner strategy demonstrated greater accuracy, and the ensemble methods regularly outperformed single CNNs. This investigation highlights how cutting-edge methods like meta-learning CNNs may improve the precision of diabetic retinopathy diagnosis.

3. DIABETIC RETINOPATHY

During the early stages of diabetic retinopathy, specific manifestations on the retina can be observed, indicating disease progression. Microaneurysms are one of the initial signs, this occurs as a consequence of pericytes' degeneration and loss, causing the dilation of capillary walls. Intraretinal hemorrhages occur when the walls of capillaries or micro aneurysms rupture. Non-proliferative diabetic retinopathy (NPDR) includes additional abnormalities like soft and hard exudates, intraretinal microvascular abnormalities (IRMA), venous beading, and venous loops or reduplication. IRMAs, characterized as large-caliber tortuous vessels, often emerge

in areas of ischemia as a response to attempted vascular remodeling. Neovascularization, characterized by the growth of new retinal vessels due to ischemia, is also a notable manifestation, distinguishing proliferative diabetic retinopathy (PDR). Fig. 1 presents an illustrative fundus image displaying these indicative lesions [6].
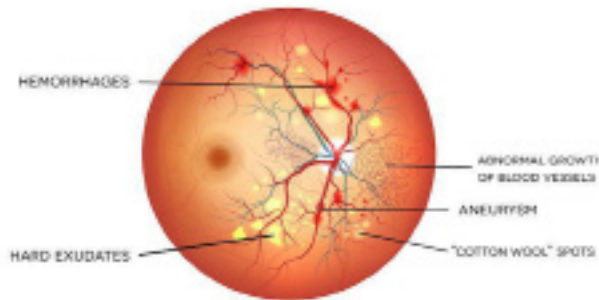
Figure 1. Diabetic retinopathy impacts on retinal blood vessels

At any stage of diabetic retinopathy, the occurrence of diabetic macular edema (DME) can significantly contribute to visual impairment. Notable abnormalities associated with DME include exudates within one disc diameter of the fovea's center, exudates within the macula, retinal thickening within one disc diameter of the fovea's center, and the presence of microaneurysms or hemorrhages within the same region. Different grading protocols have been devised to evaluate the clinical severity of diabetic retinopathy.Although the Early Treatment Diabetic Retinopathy Study (ETDRS) grading system is regarded as the gold standard, it has proven difficult to implement in everyday clinical practice. Alternative severity scales have been suggested as a result in various nations to improve patient screening and streamline communication among healthcare professionals. One such scale is the International Clinical Diabetic Retinopathy Disease Severity Scale as shown in Table 1, which classifies diabetic retinopathy into five severity levels based on specific findings observed during dilated ophthalmoscopy. These findings include the presence of microaneurysms, intraretinal hemorrhages, venous beading, intraretinal microvascular abnormalities (IRMA), and neovascularization [7].

Table 1. International Clinical Diabetic Retinopathy Disease Severity Scale

Stage	Dilated Ophthalmoscopy Observable Findings	Severity
I	No abnormalities	No DR
II	Micro-aneurysms only	Mild non-proliferative DR
III	Any of the following: - micro-aneurysms - retinal dot and blot haemorrhages - hard exudates or cotton wool spots No signs of severe non-proliferative diabetic retinopathy	Moderate non-proliferative DR
IV	Any of the following: - more than 20 intra-retinal hemorrhages in each of 4 quadrants - definite venous beading in 2 or more quadrants - prominent intra-retinal microvascular abnormality (IRMA) in 1 or more quadrants No signs of proliferative retinopathy	Severe non-proliferative DR
V	One or both of the following: - Neovascularization - Vitreous/pre-retinal hemorrhage	Proliferative DR

4. RESEARCH AND METHODOLOGY

4.1. Dataset

The Aravind Eye Hospital in rural India provided the data for the Kaggle APTOS 2019 Competition [8]. The goal was to provide reliable diagnostic tools for automated Diabetic Retinopathy Detection, giving the hospital the ability to quickly locate affected patients. The dataset consists of 5,590 DR images, which is the third-largest of its sort. It is important to note, however, that one drawback is the existence of a considerable class imbalance,particularly in the Severe NPDR class, which has only 193 photos. Aravind Eye Hospital technicians traveled to the rural areas of the country to capture the images and that's the main concern that APTOS dataset demonstrates variances brought on by various camera settings applied across many centers, much like the Kaggle EyePACS dataset does. As they were gathered in a real-world clinical scenario, the labels and data may also include noise like artifacts, focus issues, and differences in exposure (over or under) levels. The dataset is divided in 5 categories i.e 0-No DR 1-Mild 2-Moderate 3-Severe 4-Proliferative DR.

Figure 2. Classification of APTOS-2019 dataset
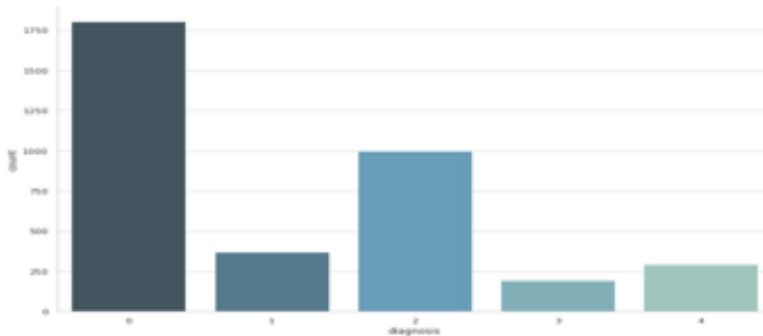
4.2. Deep learning

Deep learning is a branch of machine learning that utilizes neural networks with multiple layers to extract intricate patterns and representations from data. Inspired by the structure of the human brain, deep learning techniques rely on artificial neural networks to process and analyze complex information, enabling the model to learn and make predictions based on the extracted features. It involves automatically learning the mathematical representation of the underlying relationships within data, uncovering latent and intrinsic patterns in an automatic manner. Deep learning models easily pick up complex features by using a lot of labeled data andeasily pick up complex features by using a lot of labeled data and modifying network weights through back propagation,leading to significant advancements in artificial intelligence.

4.3. Convolutional Neural Network

With inspiration from human vision, convolutional neural networks (CNNs) are neural networks that process 2D arrays as input. They use convolution, a mathematical procedure, to take important details out of images. CNNs use filters or kernels to compute convolutions across the input data, resulting in feature maps, in contrast to traditional Deep Neural Networks (DNNs), where all neurons at a given layer contribute to the output of every neuron at the next layer. A window of pixels determined by the filter's size affects each unit in the feature map. The area in the input space that a specific CNN feature takes into account is determined by this receptive field. The convolutional part of the network is responsible for feature extraction, while the subsequent layers, often a DNN, perform classification based on the learned features.

4.4. Transfer Learning

Transfer learning describes the method of using the knowledge gained by using pre-trained models on one task to enhance performance on a related but distinct task. The goal of transfer learning is to move the learnt parameters or representations from the source task to the target task. The pre-trained model collects common patterns and features that are helpful for a variety of tasks and is often trained on a big dataset.The pre-trained model can be applied to new data more successfully and possiblyperform better than when learned from the start by adjusting or tuning it for the desired task. Transfer learning becomes very beneficial when the intended task has few labeled data points or when the target task and source task have similar properties. It aims to leverage knowledge from pre-trained models to improve performance on a related task.
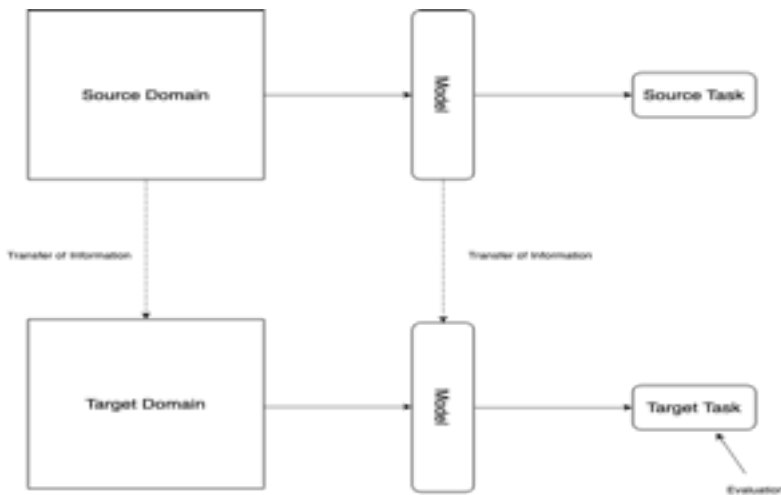
Figure 3. Basic structure of transfer learning

4.5. Meta Learning

Meta-learning, also known as learning to learn, focuses on developing algorithms or models that can learn how to learn or adapt quickly to new tasks. Meta-learning involves training a model on a distribution of tasks, where the model learns generalizable knowledge or prior knowledge that enables rapid learning on new, unseen tasks. The objective is to acquire knowledge or strategies that can be applied to new tasks, allowing the model to learn with fewer examples or adapt quickly to new scenarios. Meta-learning can involve techniques such as few-shot learning, where a

model is trained to learn from only a few examples, or meta-optimization, where the model learns to optimize its own learning process.
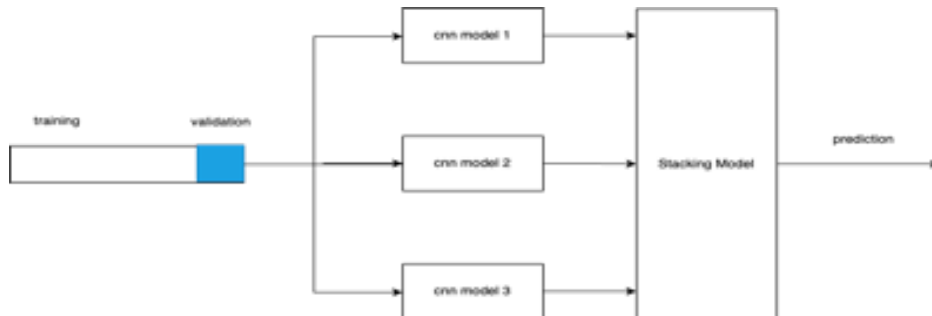
Figure 4. Basic structure of meta learning

5. IMPLEMENTATION DETAILS

5.1. Base Models

For training the stacking model in ensemble learning we first need to train and prepare the base models. After the model is trained on the dataset we use the outputs of these individual base models as the input of the stacking model. We have used only three base models for this experiment.

5.1.1. EfficientNet

EfficientNet models aim to achieve high accuracy while still using computational resources efficiently. Efficient Net-B5 has been used as the first base model. The scalable architecture of EfficientNet models makes it simple to change the model size in accordance with the resources at accessibility or your specific requirements [9].
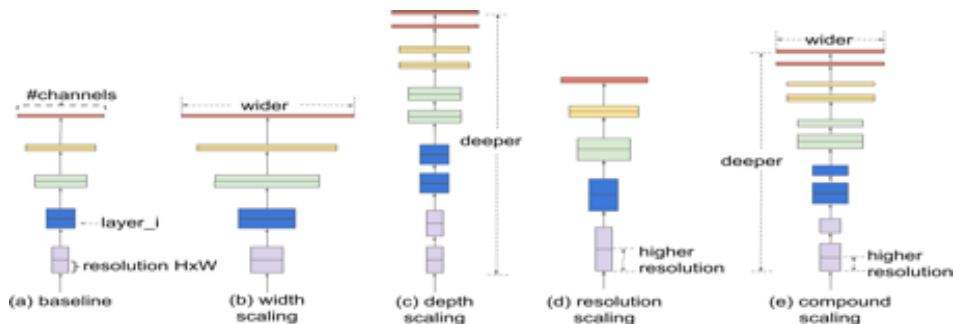
Figure 5. Basic architecture of EfficientNet

5.1.2. ResNet

ResNet models make use of residual connections to help solve the issue of training with vanishing gradients. Resnet-18 is used for the following implementation. This makes it possible to train deeper networks efficiently and raises the performance of the model as a whole. In comparison to deeper variants, ResNet18 is a relatively light network, which speeds up training and uses less computing power [9].
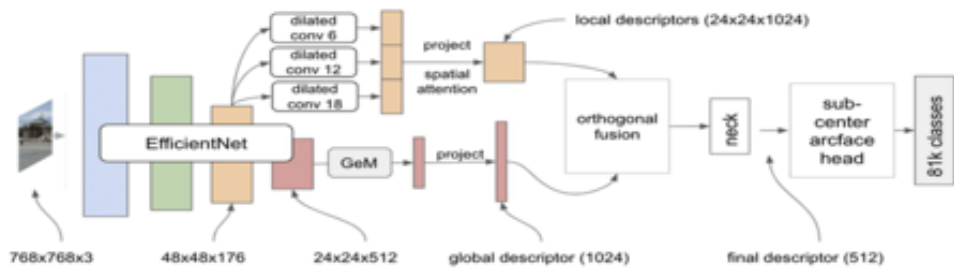
Figure 6. Basic architecture of ResNet

5.1.3. DenseNet

Each layer in a DenseNet model receives feature maps from all layers above it due to the dense connection used in these models. We have used Densenet-121 for this implementation. Better feature representations are the result of the network's dense connection, which stimulates feature reuse, enhances gradients, and encourages information flow. By promoting feature reuse and facilitating better gradient flow, DenseNet's dense connection helps prevent overfitting, which may lead to enhanced generalization [10].
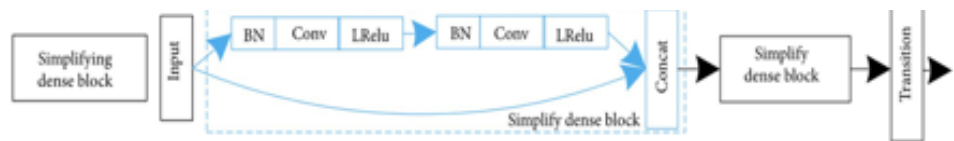
Figure 7. Basic architecture of DenseNet

5.2. Model Ensemble and Stacking

In this study, the challenge of predicting diabetic retinopathy was dealt through utilizing an ensemble of multiple deep learning models. ResNet18, DenseNet121, and EfficientNet-B5 are some of the models employed in the ensemble. By changing the final layers to correspond to the number of classes in our dataset, the mentioned three models which were originally

trained on the ImageNet dataset were customized for our specific goal. Stacking is an approach which involves combination of various machine learning models in hopes of enhancing predictive performance is the core idea behind our ensemble method. Stacking works by teaching a meta-model to base its predictions on those of a number of base models. In our scenario, a new model known as the "stacking model" was created by concatenating the outputs from these three base models.

The stacking model used in this study was a straightforward linear model. A 15-element vector is created by concatenating the outputs of the base models, each of which generates a prediction vector of length 5 (corresponding to the 5 classes in the dataset). The model is able to learn the best combination of the predictions from the basic model by passing this vector through a linear layer with five outputs. By employing this stacking strategy, the model is able to fully capitalize on the advantages of each base model, possibly leading to a more reliable and precise predictive model. The stacking model is trained using the Adam optimizer and a common loss function (in our instance, Cross Entropy Loss).

5.3. Training and Validation Split

To guarantee that the models could be properly trained and evaluated in this research, the dataset was divided into training and validation subsets. By dividing the dataset in this form, the models can be trained on one part of the data (the training set), and their performance can then be assessed on a second subset of the data (the validation set), which they were not exposed to during training. In a real-world application, this helps in estimating how well the trained models will respond to new data. This was done using pandas' sample function, which takes a sample of data at random, according to the provided code. 80% of the data was chosen for the training set since the frac parameter was set to 0.8.

The random_state parameter was set to a specific value to ensure the reproducibility of the results. It ensures that each time the code is executed, the random selection of data will be the same. After choosing the training set, the validation set was made by removing its indices from the entire dataset, thereby erasing the 20% of data that wasn't part of the training set. This type of split was used for this study on the detection of diabetic retinopathy since it is frequently used in machine learning and deep learning projects to provide a balanced approach to training and testing models.

5.4. Image Preprocessing

In the world of deep learning and computer vision, image preprocessing is an important and crucial step. It puts a huge impact on the model's performance. Using PyTorch's transformations module, a set of common preprocessing procedures were applied to the images for this project. Before being input into the models, the photographs were initially downsized to 224x224 pixels in order to ensure that they were all the same size. The photos were then transformed into tensors, the necessary input format for PyTorch models. Additionally, the photos were standardized using a particular mean and standard deviation. These parameters were used to pre-train the models on the ImageNet dataset and are typical for images in the RGB format. This normalization step is essential since it speeds up the model's convergence during training and can improve performance.

5.5. Training Process

Standard deep learning techniques were used to handle the training of the models, including the base models and the stacking model. The Adam optimization technique was used for optimizing the parameters of the models. This adaptive learning rate method uses little memory and is computationally effective. Due to its effectiveness, it has been widely used in deep learning. A common approach for multi-class problems with classification, the Cross-Entropy Loss, was used to train the models. The variation between the expected probability and the actual labels is measured by the Cross-Entropy Loss. As a result, the model is recommended to output low probability for the incorrect classes and high probabilities for the correct classes.

The main models were initially trained separately. The stacking model was then trained using the Adam optimization algorithm and Cross-Entropy Loss, and its data inputs were concatenated and used in this process. The stacking model learns to correct for errors made by the base models by training it to base its predictions on their outputs, which will enhance the accuracy of all predictions.

6. RESULTS AND DISCUSSION

6.1. Base Model Performance

In the case of the individual base models, they were evaluated using the accuracy metric, which is the proportion of correct predictions out of

the total predictions. For the EfficientNet-B5 model, the accuracy on the validation set was approximately 82.24%. The second model, ResNet18, achieved an accuracy of about 78.96% on the validation set. The third model, DenseNet121, performed comparably to the first model, with an accuracy of about 81.28% on the validation set. In general, these results suggest that all three base models were able to learn useful representations from the training data and generalize well to unseen data in the validation set. However, there were variations in their performances, and this further justifies the use of model ensemble and stacking techniques to leverage their complementary strengths and improve the overall system's

6.2. Stacking Model Training

The base models (efficientnet-b5, resnet-18, densenet-121) predictions were used to train the stacking model. The stacking model's input was a perfomance. combination of the predictions from these models. The typical method of using the original features as input (in this case, the image data) is different from this. The stacking model was trained using a standard supervised learning procedure. Binary Cross-Entropy with Logits Loss, a loss function appropriate for binary classification issues, was employed. Adam was used for training the model as its the widely used optimizer algorithm because of its effectiveness. Every 20 epochs, the loss was recorded during the 500 epochs of training in order to track its progress. The model parameters were preserved for later usage after the training.
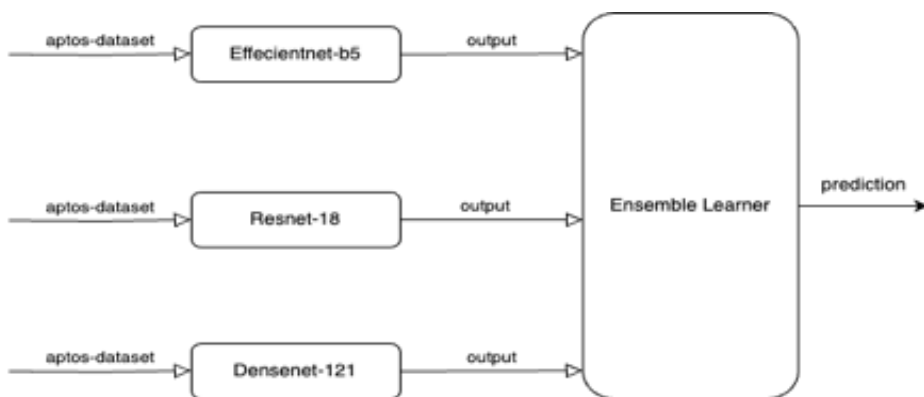
Figure 8. Base models as input for training Stacking Model

6.3. Stacking Model Performance

Multiple metrics were used to evaluate the stacking model's performance on the validation set. On the validation images, the stacking model's accuracy was 92.76%. This indicates that for approximately 93% of the photos in the validation set, the stacking model provided accurate predictions. The precision and recall score, known as the F1 score, was approximately 0.91. This shows that a decent balance between accurately detecting positive cases (recall) and reducing false positives (precision) was maintained by the stacking model.

Table 2. Showing the matrics scores of stacking model

Matrics	f1	accuracy	precision	recall	roc_auc
Score	0.92	0.90	0.90	0.91	0.92

Additionally, the precision score was approximately 0.90, indicating that the model correctly predicted positive cases 90% of the time. Recall was approximately 0.92, indicating that 92% of the positive cases in the validation set were properly identified by the model. Finally, the model's ROC-AUC score was close to 0.93, showing that it is very capable of differentiating between the classes. A high score on the ROC-AUC measure denotes a strong model in binary classification problems. These metrics indicate the effectiveness of the chosen ensemble and stacking technique overall, indicating that the stacking model performed well on the validation set
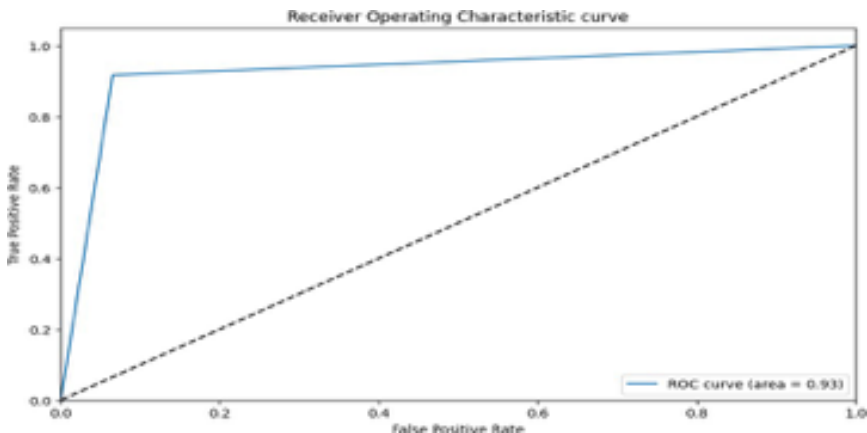
Figure 9. Showing the ROC curve area of the stacking model

7.EXPERIMENTS

7.1.Few-Shot Learning with APTOS-2019

We used few-shot learning as an experimental strategy with the APTOS-2019 dataset. This method seeks to develop models that can efficiently learn knowledge from a limited amount of data. Due to the APTOS-2019 dataset's unbalanced class distribution, the results, however, were not satisfactory. An unbalanced dataset can have a major impact on the effectiveness of a machine learning model, especially when utilizing a few-shot learning strategy that mainly relies on a tiny sample of data.

7.2.Classification Using Meta Learning Approach

Moving forward, we used the meta learning approach on the APTOS-2019 dataset for classification into multiple classes rather than binary classification. The performance of the stacking model on validation images was as follows:

Matrics	f1	accuracy	precision	recall
Score	0.833	0.833	0.835	0.833

The ROC-AUC scores were varying significantly across different classes:

Classes	Class 0	Class 1	Class 2	Class 3	Class 4
Score	0.978	0.726	0.874	0.709	0.716

The results suggest an acceptable level of performance, but there is room for improvement.

7.3.Binary Classification

After evaluating the multi-class model's performance, we modified the strategy for binary classification. This modification was developed in light of the difficulties that multi-class classification presents when dealing with imbalanced data. As a result, the findings significantly improved and the accuracy of the stacking model exceeded 90%. The experiments have demonstrated that although meta-learning and few-shot learning algorithms can be used to diagnose diabetic retinopathy, careful consideration of the class distribution in the dataset is necessary to ensure the best model performance.

8. CONCLUSIONS

8.1. Summary of Findings

This study employed deep learning techniques to classify the severity of Diabetic Retinopathy, a serious eye condition common in diabetic patients. Specifically, the study used an ensemble of pretrained convolutional neural networks (EfficientNet-B5, ResNet18, and DenseNet121) and a stacking approach to improve model performance. The base models achieved individual validation accuracies around 78% to 82%. However, the stacking model achieved a validation accuracy of approximately 93%, showcasing the effectiveness of the ensemble and stacking method. The stacking model also achieved impressive scores on other performance metrics, including precision, recall, F1-score, and ROC-AUC score, indicating its robustness in classifying the DR condition. These findings suggest that ensemble learning and stacking methods can be powerful tools in the context of medical image classification tasks, particularly when the goal is to leverage the strengths of multiple models to improve overall performance.

8.2. Potential Improvements and Future Work

Despite the promising results, there are several potential areas of improvement and directions for future work. Fine-tuning the base models on the specific task could potentially improve their individual performances and, by extension, the performance of the ensemble model. Additionally, exploring different architectures for the stacking model could lead to improved performance. Hyperparameter tuning, such as adjusting the learning rate or the number of epochs, could also yield better results. Another promising direction for future work could involve expanding the ensemble to include more diverse base models. The current study utilized models based on CNNs; including models based on different architectures, such as transformer models, could potentially increase the robustness of the ensemble.

8.3. Implications of the Study

This study has several implications, especially for the application of deep learning in the medical field. First off, it shows how deep learning models could be used to help with the identification of diseases like diabetic retinopathy. Accurate early detection can significantly enhance a patient's prognosis, resulting in better medical outcomes. Additionally, the application of ensemble and stacking methods demonstrates how

we can capitalize on the complementing qualities of diverse models to enhance overall performance, a strategy that can be used in a variety of other healthcare situations. The study additionally emphasizes the value of ongoing model validation and evaluation to make sure the model works effectively on both training and real-world data. This is essential in the medical field because misdiagnosis may be quite expensive and the stakes are so high.

REFERENCES

[1]Atwany, M.Z.; Sahyoun, A.H.; Yaqub, M. Deep learning techniques for diabetic retinopathy classification: A survey. IEEE Access 2022, 10, 28642–28655.w

[2]Amin, J.; Sharif, M.; Yasmin, M. A review on recent developments for detection of diabetic retinopathy. Scientifica 2016, 2016, 6838976.

[3]Sarki R, Ahmed K, Wang H, Zhang Y. Automated detection of mild and multi-class diabetic eye diseases using deep learning. Health Inf Sci Syst. 2020 Oct 8;8(1):32. doi: 10.1007/s13755-020-00125-5. PMID: 33088488; PMCID: PMC7544802.

[4]T. Nazir, M. Nawaz, J. Rashid, R. Mahum, M. Masood, A. Mehmood, F. Ali, J. Kim, H.-Y. Kwon and A. Hussain, Detection of diabetic eye disease from retinal images using a deep learning based CenterNet model, Sensors, vol.21, no.16, DOI: 10.3390/s21165283, 2021.

[5]Enkvetchakul, Prem & Surinta, Olarik & Noppitak, Sangdaow. (2022). Effective Data Resampling and Meta-learning Convolutional Neural Networks for Diabetic Retinopathy recognition. ICIC Express Letters, Part B: Applications. 13. 939-948. 10.24507/icicelb.13.09.939.

[6]https://www.eyeops.com/contents/our-services/eye-diseases/diabetic-retinopathy.

[7]https://www.researchgate.net/publication/326854068_Diabetic_Reti-nopathy_Stage_Classification_Using_Convo lutional_Neural_Networks.

[8]https://www.kaggle.com/c/aptos2019-blindness-detection.

[9]Tan, M. & Le, Q.. (2019). EfficientNet: Rethinking Model Scaling for Convolutional Neural Networks. Proceedings of the 36th International Conference on Machine Learning, in Proceedings of Machine Learning Research 97:6105-6114 Available from https://proceedings.mlr.press/v97/tan19a.html.

[10]Gao Huang, Zhuang Liu, Laurens van der Maaten, Kilian Q. Wein-berger; Proceedings of the IEEE Conference on Computer Vision and Pattern Recognition (CVPR), 2017, pp. 4700-4708.

[11]Gao Huang, Zhuang Liu, Laurens van der Maaten, Kilian Q. Wein-berger; Proceedings of the IEEE Conference on Computer Vision and Pattern Recognition (CVPR), 2017, pp. 4700-4708.

[12] Ramzan, Farheen & Khan, Muhammad Usman & Rehmat, Asim & Iqbal, Sajid & Saba, Tanzila & Rehman, Amjad & Mehmood, Zahid. (2019). A Deep Learning Approach for Automated Diagnosis and Multi-Class Classification of Alzheimer's Disease Stages Using Resting-State fMRI and Residual Neural Networks. Journal of Medical Systems. 44. 10.1007/s10916-019-1475-2.

Analysis and Design of RFID Antenna Based on Broadside-Coupled SRR

Amina Bendaoudi[1], Mohamed Debab[2], Mohammed Berka Zoubir Mahdjoub[3]

[1]*Department of Mechanical Engineering, Ozyegin University, Istanbul, Turkey*

[2]*Department of Mechanical Engineering, Ozyegin University, Istanbul, Turkey, layth.ismael@ozu.edu.tr, ORCID: 0000-0002-1850-3998*

[3]*Department of Materials Engineering, University of Technology, Baghdad, IRAQ, 130006@uotechnology.edu.iq*

ABSTRACT

This Paper Presents A New Structure Of Circular Patch Antenna With Slots That Operate In Rfid Applications Microwave. Additionally, It Utilizes Broadside-Coupled Complementary Split Ring Resonator (Bc-Srr) In The Ground Plane In Order To Obtain An Rfid Antenna Technology That Operates Around 2.45 Ghz And 5.80 Ghz. The Circular Patch Antenna Is Composed Of An Arlon Ad430 Substrate With The Dielectric Permittivity Of 4.3, Loss Tangent Of 0.003, And Thickness Of 5Mm. The Parameters Examined In This Paper Are The Resonant Frequency, Reflection Coefficient, And The Radiation Pattern Of The Proposed Antenna. The Results Obtained By Ansoft Hfss Were Compared To Those Obtained By Cst Mws (Computer Simulation Technology-Micro Waves Studio).

Keywords: *Radio Frequency Identification; Complementary Broadside Coupled SRR resonators; Metamaterial; Circular patch.*

1. INTRODUCTION

Recently, antenna researchers worldwide have been attracted by the single/double negative metamaterials, also called zero-index materials, due to their peculiar properties. These artificially engineered homogeneous media provides unusual and useful phenomenon due to their controllable electric and magnetic responses [1]. Metamaterial is artificial metallic structures having simultaneously negative permittivity and permeability, and consequently, have a negative index of refraction. It gains its properties from structure rather than composition [2]. The first researches concerning the properties of metamaterials are made by Victor Veselago in 1968. Later Smith [3] implements first left-handed materials consist of periodic split-ring resonators (SRR's) and long strips [4].

The metamaterial structures that are used for improving patch antenna performance are Split Ring Resonators (SRR) or the Complementary Split Ring Resonator (CSRR) [5].

An RFID, Radio Frequency Identification, system is generally composed from a reader, and one or more transponders or tags. The communication between the reader and the tag is achieved by modulated backscattering of the reader's carrier wave signal [6]. In 1990, RFID became prevalent in many industry services, such as access control, document tracking, distribution logistics, automotive systems, and animal tracking [7]. The RFID system is used in many applications as access control, logistic, bank, health, and transport [6].

The microstrip patch antennas generally meet most of these requirements and hence, have better prospects than conventional antennas [8]. They are famous to be low profile, low weight, ease of fabrication, conformable to planar and non-planar surfaces and mechanically robust [6]. The studies have focused very quickly to the development of filters, phase shifting and antenna with new performance one of the promising applications in the field of antenna design is metamaterial antennas [9].

This paper is focused on the use the magnetic resonator called Broadside Coupled SRR "BC-SRR" should therefore eliminate the magneto-electric coupling so the E field does not respect the symmetry of the structure.

Wang et al. proposed tuning the electromagnetic response in the microwave region through subunit-cell relative displacements between the two layers comprising a broadside coupled SRR (BC-SRR) structure under magnetic excitation [10].

A circular patch antenna is being widely used in RFID technologies and other microwave applications. Use of BC- SRR helps in improving various properties and to overcome the drawbacks of patch antennas, such as increasing radiation efficiency and providing the good adaptation of antenna. We propose a modification in conventional antenna geometric by introducing slots in the circular patch with a ground plane periodically etched by BC-SRR.

2. THEORY

Antenna Design

Concept of Broadside Coupled Split Ring Resonator (BC-SRR)
The equivalent circuit model of the SRR shows that the capacitive gaps in the structure are of the greatest importance in determining its resonance frequency [11]. The SRR dimensions will decide the notch frequency. The strong magnetic coupling of propagating electromagnetic field from SRR will suppress the radiation at notch frequency [12].

(a)   (b)
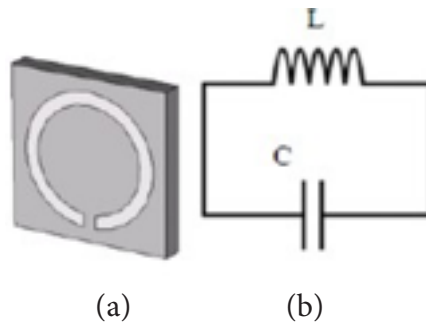
Figure 1. Topology of the Split Ring Resonator (a) SRR resonator cell proposed, (b)Equivalent resonant curcuit.

The split rings are coupled by means of a strong distributed capacitance in the region between the rings (the slots are meaningfully wider than the distance between the rings). The BC-SRR is shown in Fig.2 [13].
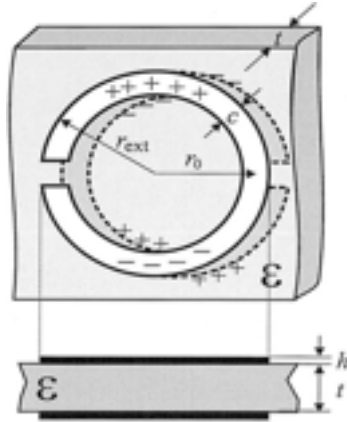
Figure 2. Broadside coupled SRR (BC-SRR).

The whole device then behaves as a circuit driven by an external electromotive force. The total capacitance of this LC circuit will be the series capacitance of the upper and the lower halves (with respect the line containing the ring gaps) of the SRR and the resonance frequency w0 is given by [13]:

$$\omega_0 = \sqrt{\frac{2}{\pi r_0 L C_{\text{pul}}}} \qquad (1)$$

where is the per unit length Cpul capacitance between the rings, L is the total inductance of the SRR, and r0 is the average radius of the considered SRR. The analysis of the BC-SRR can be simplified by neglecting of the cross-polarization effects so, the resulting equations can be summarized as follows [13]:

$$m_z = \alpha_{zz}^{mm} B_z^{\text{ext}} \qquad (2)$$

$$p_y = \alpha_{yy}^{ee} E_y^{\text{ext}} \qquad (3)$$

$$p_x = \alpha_{xx}^{ee} E_x^{\text{ext}} \qquad (4)$$

The BC-SRR polarizabilities have been obtained in a self-consistent way, they can be used in a local field theory in order to determine the macroscopic constitutive parameters of media consisting of a regular array of SRRs. This local field theory makes use of the well-known Lorentz theory [13].

The configuration of the proposed patch-slot circular antenna is illustrated in Fig.3. Its structure is based on an Arlon AD430 dielectric substrate which has permittivity of 4.3 and height h=5mm. The characteristics impedance of coaxial cable 50ohm has matched with the input impedance of the conventional patch antenna. The resonance frequency is fr = 3.65GHz [14].
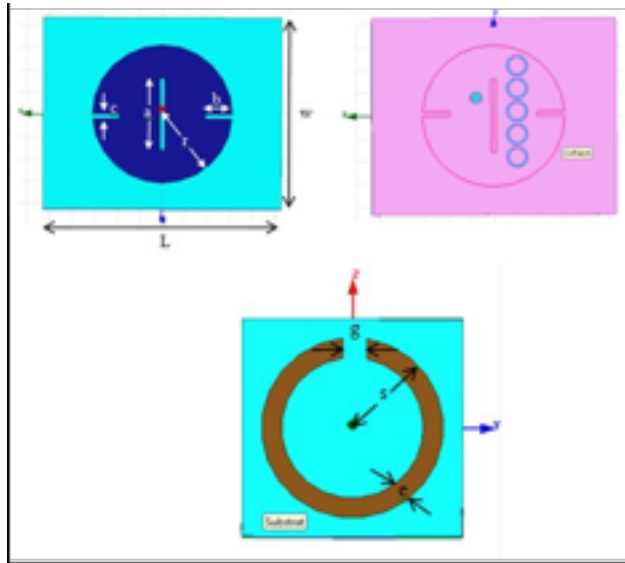
Figure 3. Layout of the proposed antenna.

The proposed antenna consists of antenna with ground plane periodically etched CSRR. The complementary SRR must produce a negative effective permeability around the resonant frequency of the antenna. The network is homogeneous and periodic that contains five SRRs circular with a periodicity to order 1mm. The dimensions of the patch-slot circular antenna are tabulated in Table 1. The geometrical dimensions of the BCSRR unit cell are; radius of the split ring s=2.3 mm, width of the rings e=0.5mm and gap at the split of ring is g=0.5 mm. The dimensions of circular split ring resonator are chosen in such a way that it resonates at the same frequency as that of the proposed antenna.

Table 1. Dimensions Of The Patch-Slot Circular Antenna.

Parameters	W	L	h	a	b	c	r
Values (mm)	43	53	5	16	6	1	16

3. RESULTS AND DISCUSSION

HFSS tool was used as a platform to design of the antenna, to match the radiation parameters as, input impedance, return loss, gain, directivity and radiation pattern. The obtained results have been compared to those obtained by CST.

Antenna in the absence of slots and CSRR
The simulated S-parameters result is illustrated in Fig.4.
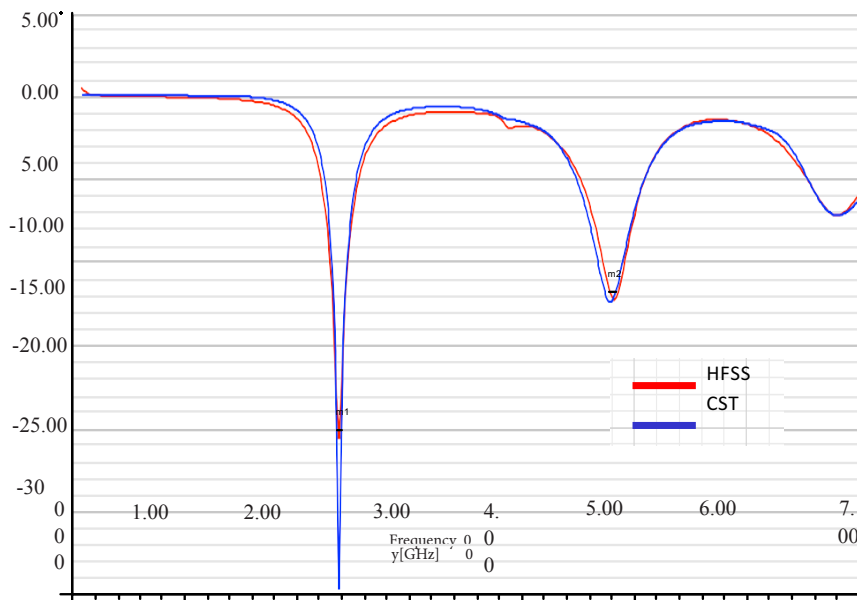
Figure 4. Reflexion coefficient of the antenna without slot.

It can be seen from this figure that, the circular patch antenna without slot and without CSRR has a double resonance. Based on the results given by HFSS, the first resonance at 2.38 GHz, with S11=-20 dB and the second at 4.82 GHz with S11= -12.68 dB. From the results given by CST, the first resonance at 2.38 GHz, with S11=-29.20 dB and the second at 4.78 GHz with S11= -12.70 dB.

The simulated radiation patterns result is illustrated in Fig.5.

(a)

(b)
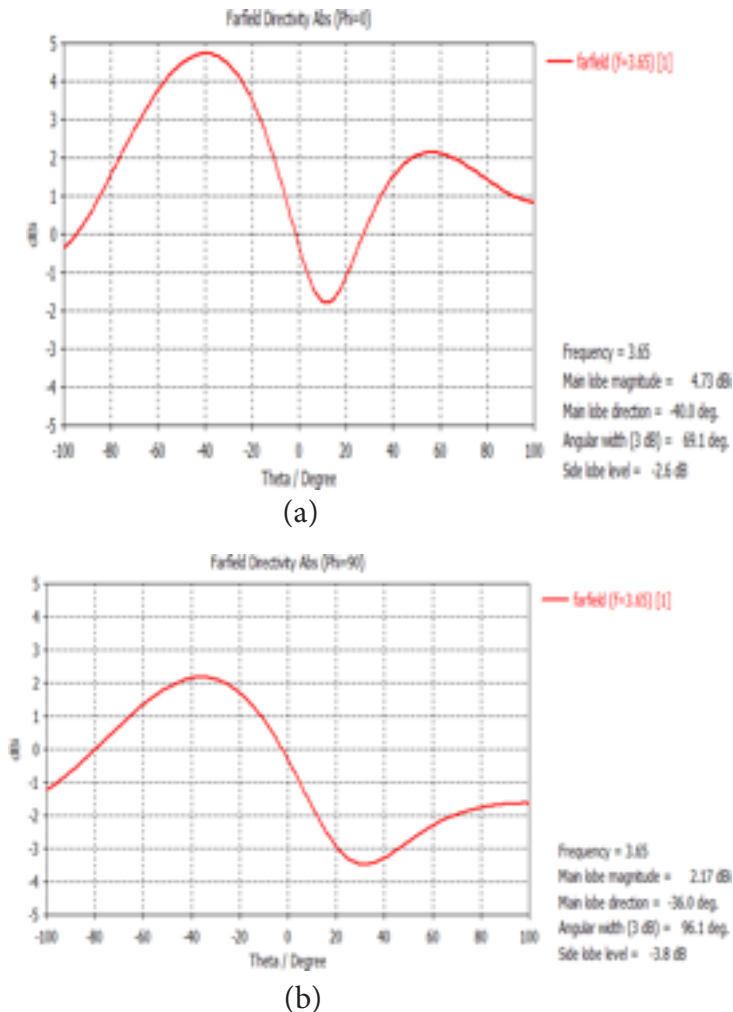
Figure 5. Simulated Gain by CST, (a) for Phi=00 (b) for Phi=900.

From the results given by CST, the maximum directivity attained by the antenna is 2.17 dB and the maximum gain of
4.73 dB. HFSS tool was used as a platform to design of the proposed antenna (Figure 4), to match the radiation parameters as, reflexion coefficient, gain and radiation pattern. The obtained results have been compared to those obtained by CST.
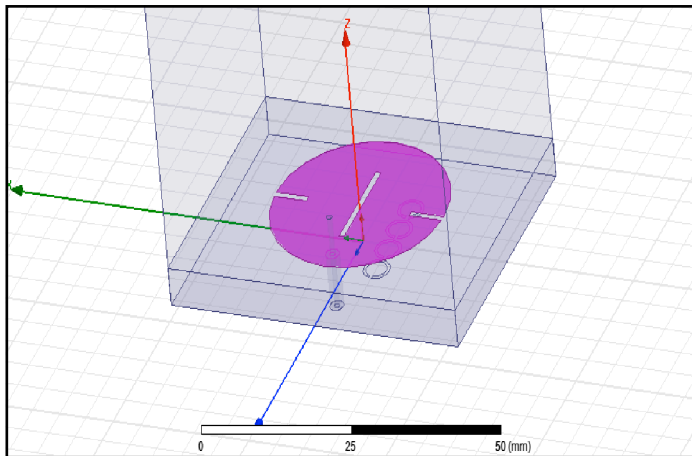
Figure 6. Simulation model of proposed antenna by HFSS.

Antenna in the presence of slots and CSRR
The simulated S-parameters results are illustrated in Fig.7.

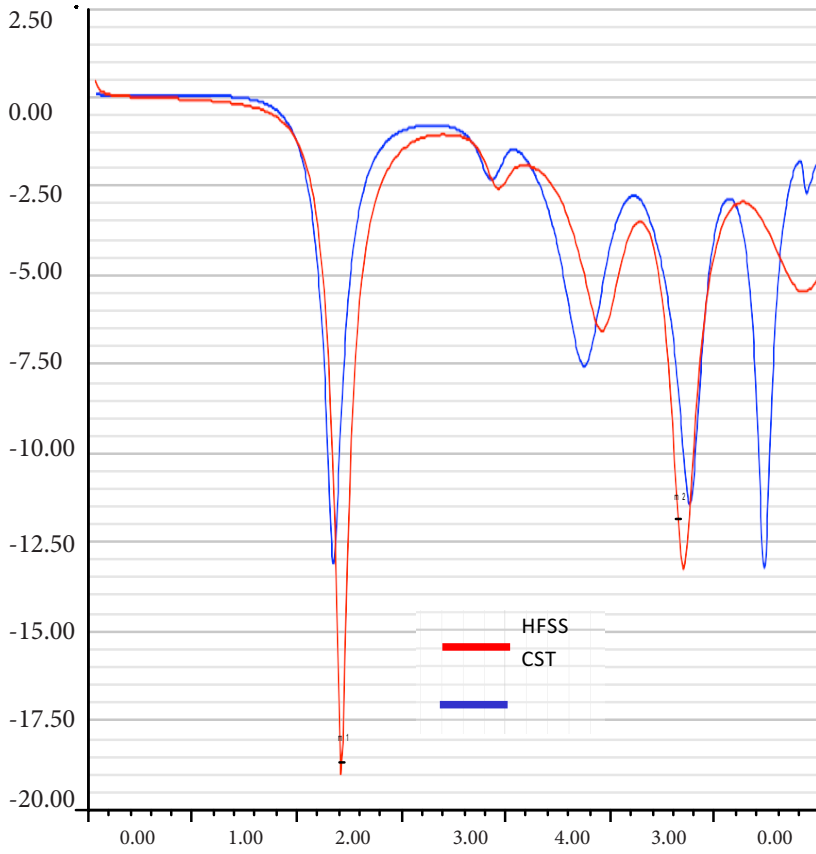**Figure 7.** Illustrate the radiation patterns around 2.45 GHz and 5.80 GHz at E-plane and H-plane respectively.
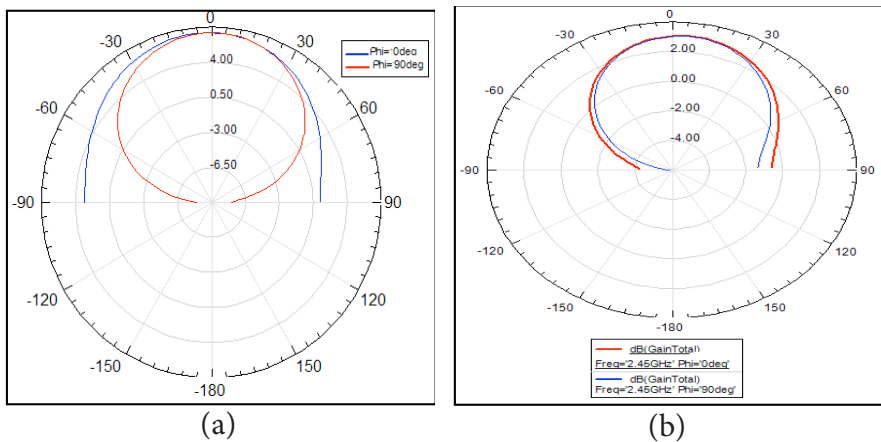

(a) (b)

Figure 8. Realized radiation pattern at 2.45 GHz (a) by HFSS and (b) by CST

We notice slight difference between the results obtained by the HFSS simulator and those obtained by CST in terms of the resonance frequency, the antenna impedance, and the gain. This difference is due to the meshing technique used during the simulation and to the numerical method of each simulator uses.

Table 2. Comparison Of Parameters Result Of Circular Antenna With And Without Slot AnBC-SRR.

	Conventional antenna		Proposed antenna	
	HFSS	CST	HFSS	CST
Optimal frequency (GHz)	2.38	2.38	2.44	2.41
	4.82	4.78	5.66	6.50
Reflection coefficient (dB)	-20	-29.20	-19	-13.08
	-12.68	-12.70	-13.50	13.40
Gain (dB)	/	4.73	3.08	6

From the comparison table 2, the results indicate that the BC-SRR resonator has an effect on the conventional antenna by shifting the frequency regions to a different value as well as affecting the S11 parameters. Thus multiband operation is achieved by coupling two BCSRR units having selected parameters with the circular patch. It has been concluded that the association between BC-SRR and the slot leads to an improvement in terms of the bandwidth and the gain.

4.CONCLUSION

The present work reports the development of a multiband circular patch antenna by utilizing Broadside Coupled Split Ring Resonator (BCSRR) units. Split ring resonator array is used to produce the negative magnetic permeability. This antenna makes use of the resonant property of metamaterial BCSRR units for multiband frequency designing. Since the magnetic resonant frequency of the BCSRR depends on the effective capacitance and inductance of its rings. The radiating frequencies can be designed to other desired values by making changes in dielectric thicknesses and in ring parameters. The multiband frequency operation in antenna based on BCSRR is manifested and the results presented and simulated by using: HFSS and CST. The results indicate that the metamaterial has an effect on the conventional circular patch antenna by shifting the frequency regions to a low-value where the structure will be able to ameliorate

performance in terms of reflection coefficient and radiation patterns in both the H-plane and E-plane. The antenna presents good performances. This antenna system is suitable for RFID applications microwaves.

REFERENCES

[1]   Jamal MR. ''A Proposed Design of Unit Cell of Metamaterial for 5G Mobile Communication''. TELKOMNIKA. Vol 15(3): pp1145–1148 , 2017.

[2]   Smith, D., Padilla, W., Wier, D., Nemat-Nasse, S., Schultz, S.: ''Composite medium with simultaneously negative permeability and permittivity''. Phys. Rev. Lett. Vol 84, pp 4184–4187, 2000.

[3]   A.Bendaoudi, Z. Mahdjoub,''Comparative study of patch antenna loaded with slot split-ring resonators on different substrate materials. Photonic Network Communications'', Vol 35, pp195-203, 2018.

[4]   A.Bendaoudi, Z. Mahdjoub, ''Regular paper Performance Enhancement of Rectangular Patch Antenna by Loading Complementary Multi-Ring SRR''. J. Electrical Systems Vol 14(1), pp143-155, 2018.

[5]   M. Ihamji LASTI E. Abdelmounim LASTI, H. Bennis, M. Lotfi, M. Latrach: "A New Design of a Miniature L- slot Microstrip Antenna for RFID Tag", Conference ICCWCS'17, November 2017, Larache, Morocco.

[6]   Mahdi Abdelkarim, Seif, Lassad Larach, Ali Gharsallah; "Improvement of the Frequency Characteristics for RFID Patch Antenna based on C-Shaped Split Ring Resonator". International Journal of Advanced Computer Science and Applications, Vol. 9, No. 2, 2018.

[7]   Chirag arora1 , shyam s. pattnaik2 and rudra narayan baral:'' Metamaterial inspired DNG superstrate for performance improvement of microstrip patch antenna array''. International Journal of Microwave and Wireless Technologies, 2018.

[8]   E. Ekmekci, A. C. Strikwerda, K. Fan, G. Keiser, X. Zhang, G. Turhan-Sayan, and R. D. Averitt ; "Frequency tunable terahertz metamaterials using broadside coupled split-ring resonators". Phys. Rev. B 83, 193103, 2011.

[9]   Seif Naoui, Lassaad Latrach, Ali Gharsallah ; "RFID Antenna by Using Metamaterials With Negative Effective Permeability". 978-1-4799-8172-4, 2015 IEEE.

[10]   S.CHAKRABARTI and S.ANANTHA RAMAKRISHNA, "From effective medium dispersion to photonic band gaps".. Pramana – J. Phys., Vol. 78, pp. 483–492, 2012.

[11]   Madhav M. Venkateswara Rao1, T. Anilkumar, "Conformal Band Notched Circular Monopole Antenna Loaded with Split Ring Resonator B. T. P". Wireless Pers Commun, Vol.103, Issue 3, pp 1965–1976, 2018.

[12]   Ricardo Marqués, Francisco Mesa, Jesús Martel, Francisco Medina ; "Comparative Analysis of Edge- and BroadsideCoupled Split Ring Resonators for Metamaterial Design—Theory and Experiments". IEEE TRANSACTIONS ON ANTENNAS AND PROPAGATION, VOL. 51, NO. 10, 2003.

[13]   Arshad Wahab, Jiadong Xu: "U-slot Circular Patch Antenna for WLAN. Application". TELKOMNIKA Indonesian Journal of Electrical. Engineering Vol 14(2), pp 323-328, 2015.

Cardiovascular Disease Prediction Using Artificial Intelligence

Ayodele Martin Dossou,[1] Prof. Dr. Ali Okatan[2]

[1]Prof. Dr. at Department of Civil Engineering, Istanbul Arel University,

Istanbul, mehmetfatihaltan@arel.edu.tr

[2]Department of Civil Engineering, Istanbul Aydin University, Istanbul,

hakkicanalcan@stu.aydin.edu.tr
ORCID: 0000-0002-1329-61760000-0002-1329-6176

ABSTRACT

The likelihood of contracting a disease rises with the size of the human population. Globally, there are numerous ailments, and one of the main issues facing hospital systems today is the lack of technology to detect illness in patients. Cardiovascular disease, or CVD, is one such illness. Any cardiovascular, vascular, or blood vessel ailment is referred to. More people globally die from CVDs than from any other cause, according to the WHO. More so in low- and middle-income nations. When ill, it can be quite difficult for persons who live alone to contact the hospital. As a result, we created a model that can recognize when a patient is ill and send a report to the hospital. Currently, the system merely detects and informs the hospital about patients with heart disease. We chose to focus on heart disease detection because it's one of the worst diseases and there's a significant chance that people may pass away from it. Predicting whether a patient has cardiac disease or not is a categorization issue. We consider several variables, including age, blood sugar level, cholesterol level, and many more, and then we provide the result based on the input.

Keywords: Cardiovascular Disease, Heart Disease Detection, Illness Recognition, Hospital Reporting, Categorization.

[1]Department of AI & Data Science, Istanbul Aydin University, Istanbul, mammarkhan@stu.aydin.edu.tr

[2]Prof. Dr. at Department of AI & Data Science, Istanbul Aydin University, Istanbul, aliokatan@aydin.edu.tr,ORCID: 0000-0002-8893-9711-0

1. INTRODUCTION

The research primarily focuses on the numerous category segregation techniques used to forecast cardiac disorders. A poor lifestyle, drinking alcohol, eating a lot of fat, triggering hypertension, and not getting enough exercise all contribute to heart disease. The heart of a human controls blood flow throughout the body. The majority of the human body is made up of it. Heart irregularities are a severe cause for concern because they have an impact on many different body organs. Heart illness can be thought of as irregularities or abnormalities in how the heart usually beats. Heart congestion and disease are the primary causes of the majority of fatalities in today's fast and busy environment. [1] The WHO estimates that more than 10 million people worldwide pass away each year as a result of heart disease. The only strategies to stop heart-related illnesses are through early identification and a healthy lifestyle. Today's world makes it exceedingly challenging for hospitals to provide individualized care to every patient in need because of the growing population. In light of this, we have decided to try to notify the hospitals when a patient has an illness. We generally concentrate on heart illness [2] because there is a very high possibility that a patient would suffer a serious injury or pass away as a result of it. Additionally, it shortens the time it takes to detect cardiac disease. This initiative is crucial because, if a patient is living alone and suffering from heart illness, he may not be able to ask the hospital staff for assistance. Our effort goes a long way towards assisting such people. We faced difficulties and hurdles because we lacked sufficient data sets to produce pleasing results, which we overcame by producing synthetic data. To train the algorithm and determine if the patient is ill or not, we employ machine learning modules. Even if our experiments produced solid results, we still need to put the system into practice, which means creating an app that collects patient data and sends the output to hospitals Future implementation of this is possible.

Cardiovascular detection using deep learning has been a widely researched topic in recent years. Several research studies have been conducted to investigate the feasibility and accuracy of using deep learning models for cardiovascular disease detection. Some of the related works in this area are:

"Cardiovascular Disease Detection Using Deep Learning: A Review" by Liang et al. [4] (2020): This paper provides a comprehensive review of the recent advancements in cardiovascular disease detection using deep learning. The authors discuss the different types of cardiovascular diseases and the deep-learning techniques used to detect them. They also provide an overview of the datasets used in these studies and the performance metrics used to evaluate the models."Automated Detection of Cardiovascular Disease Using Deep Learning Techniques" by Attia et al. (2019): This study [5] used a convolutional neural

network (CNN) to classify patients with and without cardiovascular disease based on their echocardiogram images. The authors achieved an accuracy of 80.8% in detecting cardiovascular disease, which outperformed the accuracy of traditional machine learning models. "Cardiovascular Disease Prediction using Deep Learning Algorithm" by Gupta et al. (2020): In this study [6], the authors used a deep learning model to predict cardiovascular disease based on demographic, lifestyle, and medical history data. The authors achieved an accuracy of 88.23% in predicting cardiovascular disease, which was higher than the accuracy of traditional machine learning models. "Deep Learning-based Detection of Cardiac Arrest Using ECG Signals" by Singh et al. (2021): This study [7] used a deep learning model to detect cardiac arrest using electrocardiogram (ECG) signals. The authors achieved an accuracy of 98.6% in detecting cardiac arrest, which outperformed the accuracy of traditional machine-learning models. M. V. Kamath et al., "Biomarkers in cardiovascular disease: Prospects for personalized diagnosis and treatment."[9] This review article examines the use of biomarkers for cardiovascular disease early detection, risk assessment, and individualized care. S. K. White et al., "Cardiac Magnetic Resonance Imaging in the Detection of Cardiovascular Disease,"[10] This study assesses the effectiveness of cardiac magnetic resonance imaging (MRI) as a non-invasive diagnostic technique in the detection and diagnosis of cardiovascular illness. Y. Wang et al., "Mobile health applications for the detection and management of cardiovascular disease." The [11] use of mobile health applications for cardiovascular disease detection and management are covered in this review article, including tracking medication compliance, monitoring symptoms and vital signs, and offering individualized treatment suggestions. "Early detection of cardiovascular disease using machine learning techniques on electronic health records: a systematic review" by M. S. Khan et al.[12] This systematic review evaluates the effectiveness of machine learning techniques in detecting cardiovascular disease using electronic health records and highlights the potential for improving early detection and personalized treatment Theresa Prince, R., et al. (2016) conducted a review of the various heart disease prediction models. Theresa employed Naive Bayes and Neural Networks as her categorization methods.

Decision tree, KNN network, and LR. All of the models' accuracy scores were compared, and the comparison process was effective [3]. Overall, these studies demonstrate the potential of deep learning models in cardiovascular disease detection and highlight the need for further research in this area.

2. PROPOSED SCHEME AND DATASET DETAILS

2.1. DATASET

The study aims to detect and diagnose cardiac disease using two datasets and utilizing nine classification methods.

2.1.1. Cardiovascular Disease Dataset

Heart disease was identified and detected using the cardiovascular disease dataset in this study, and the findings were compared to those of earlier studies. It has a lot of patient information, including medical records. Kaggle's dataset was gathered from three sources, and they are examining the findings of several medical tests, Objective reflects the information provided by the patient, and Subjective represents the data gathered as facts about cardiovascular illnesses. The set of data used for training, testing, and validation. The website contains the intended data, which is open to the public [10].

The shape of the cardiovascular diseases dataset is (68783, 12), and it is a clean version of the CVD dataset as follows:

Age - integers (unit - day)

- Height - integers (unit - cm)
- Weight - float (unit - kg)
- Gender - categorical code
- Systolic BP - integer
- Diastolic BP - integer
- Cholesterol - integer, 1: normal, 2: high, 3: Fatal
- Glucose - integer, 1: normal, 2: High, 3: Very High
- Smoking -Boolean • Alcohol intake - Boolean
- Phy activity - Boolean
- Traget – Boolean

Table 1. cardiovascular diseases dataset

Features	Descriptions
Age	The patient age in years
Gender	Gender of patient (1: Male, 0: Female)
Height	Representing the height of patient's
Weight	Representing the weight of patient's

Systolic BP	Systolic blood pressure
Diastolic BP	Diastolic blood pressure
Cholesterol	The Cholesterol Level in the blood (1: normal, 2: above normal, 3: well above normal)
Glucose	Categorical value of the sugar blood level (1: normal, 2: above normal, 3: well above normal)
Smoke	Smoking (0: No, 1: Yes)
Alcohol	Alcohol intake (0: No, 1: Yes)
Physical_Activity	Physical activity type
Cardio_Disease	Target value measuring the Presence or absence of cardiovascular disease.

Table 2. Class Distribution CVD

Class	Counts
0	35021
1	34979

2.2. How Cognitive Biases Impact User Decision Making in HCI?

35,021 out of 70,000 cases in this dataset are labelled as having no cardiovascular disease, and 34,979 cases are labelled as having cardiovascular disease. This suggests that the dataset is roughly balanced

2.3. Exploratory data analysis:

Initial data analysis is the process of looking for patterns and identifying abnormalities in data using summary statistics and graphical representation

Cleaning:

We eliminate all of the duplicate and Nan values from the data set. We see that the dataset has certain inconsistencies, such as the minimum age of 29 years and the minimum weight of 10 kg. In several circumstances, the systolic blood pressure was greater than the diastolic blood pressure. To remedy the inaccuracies, we, therefore, eliminate the outliers.

Outliers are data mistakes that have the potential to seriously skew the outcome. After cleaning the data, the box plot in the following graph demonstrates that there are no datasets where the systolic pressure is higher than the diastolic pressure. We noticed that while the dataset we used did not have any Null values, it did contain duplicate entries.

As a result, we eliminate the 24 duplicate values from the dataset to create a dataset with 60118 data points.

Correlation:

All of the features' correlation matrices, which depict how strongly one feature is connected with another, have been plotted. By doing this, we can identify any features that can skew the results and get rid of them. We can see from the correlation matrix below that age and cholesterol have a significant impact on the result.
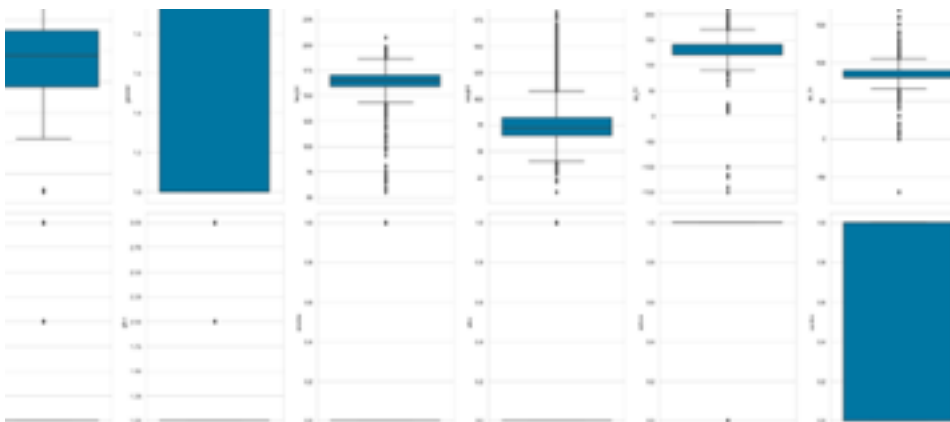

Figure 1. Box Plot confirming the removal of Outliers

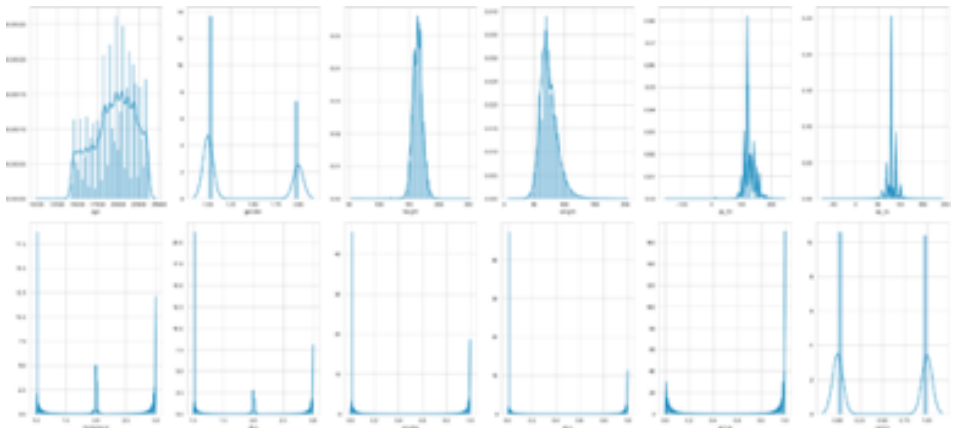**Figure 2**. Figure 2. Correlation Matrix before Feature Engineering

Figure 3. Histograms show the distribution of each feature

Feature Engineering:

The Body Mass Index (BMI) was determined during the data processing phase to assess the patient's health. A normal BMI is between 18 and 25, while an unhealthy BMI is over 25 or under 18. The formula below is used to compute the BMI values. The features for height and weight were then eliminated.

$$BMI = \frac{Weight\ (Kg)}{Height\ (Cm)}$$

The American Heart Association (AHA) claims that the systolic and diastolic blood pressure readings. There are five gradations of severity for it. Each record's blood pressure was calculated, and the level was indicated.

Feature Selection:
Based on the features' relevance, we choose them [13]. The models' accuracy is unaffected by the pertinent features. As a result, we use a correlation matrix to choose relevant data. Gender is the factor that is least connected with the target, according to the correlation matrix, which also shows that features like BMI , weight, glucose, height, smoking, alcohol use, and activity level do not have high correlations with the target. As a result, we eliminate characteristics like BMI, weight, glucose, gender, height, and alcohol and/or drug use.

Feature Scaling:
The entire feature set in the data set can be normalized using this technique [14]. The model frequently has a tendency to favor larger values when we have a characteristic with a very high value. For the feature scaling, we used the Standardization formula.

3. RESEARCH METHODOLOGY

The Gradient Boosting, Decision Tree (DT), Logistic Regression, and Neural Network algorithms will all be used in this study to classify data (NB). In order to discover the best classifier, it is also necessary to create a deep network and assess the effects of different optimization learning techniques on the detection of cardiovascular illnesses.
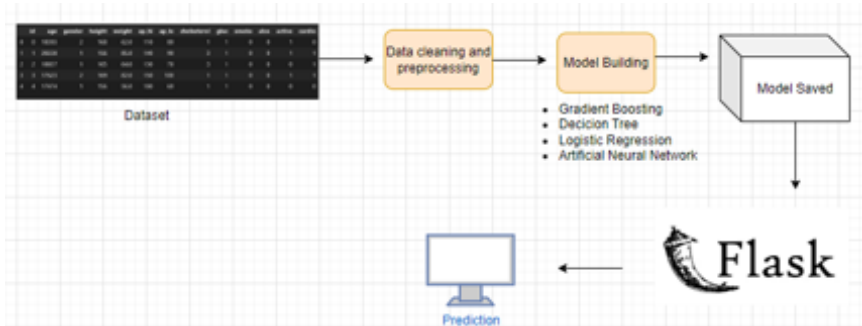
Figure 4. Below outlines how this research was conducted

3.1. The Gradient Boosting

Gradient boosting [13] is one type of boosting method. Boosting is a method for combining all the weak students to create strong students. Weak learners are characteristics in this scenario that are unable to categorize a data point on their own. The predictions made by each weak learner are used, and the category is assigned based on the results we get by applying the great majority of the forecasts made by the weak learners. A part of the boosting method is ensemble learning. Due to the ensemble method, the machine learning model performs better when multiple learners are merged. The use of sequential ensemble learning is encouraging. The model gives weight to the erroneously classified data points until it assigns the correct categorization.

3.2. Artificial Neural Network

The human brain, which has remarkable processing power due to its network of [14] interconnected neurons, serves as the model for artificial neural networks (ANN). ANNs are created utilizing a fundamental processing unit called a perceptron. The single-layer perceptron algorithm solves problems that may be divided into linear segments. Multilayer Perceptron Neural Network (MLP) can be used to solve issues that cannot be resolved linearly. There are many layers in MLP, including input, hidden, and output layers.
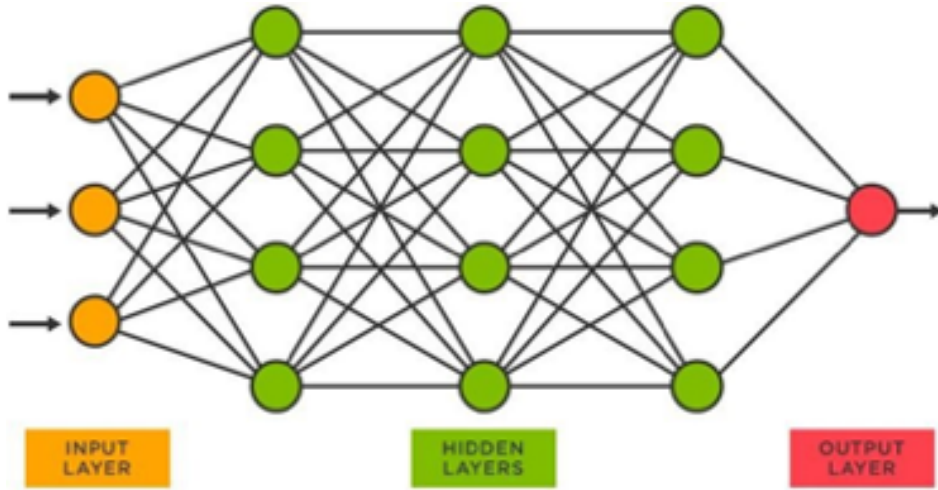
Figure 5. Artificial Neural Network architecture

To predict the cardiovascular disease, the recommended multilayer perceptron neural network was developed. The proposed ANN is composed of three layers: the input layer, the hidden layer, and the output layer.

•The Input Layer
13 neurons in all were proposed for the input layer. It was agreed that there would be an equal number of neurons and attributes in the data set.

•The Hidden Layer
Three neurons were expected to be present in the Hidden Layer. This number was selected as the starting point. By comparing their performances and then choosing the best one, the number was adjusted by raising it one at a time until it reached the number of input layer neurons. This method is based on one of the best practices for machine learning, which states that the number of neurons in the hidden layer should be equal to the sum of the neuron counts in the input and output layers.

•The Output Layer
The architecture of the Output Layer includes two neurons. The proposed NN is a classifier that runs in machine mode and outputs a class label, such as "Disease Presence" or "Disease Absence". The choice to employ two neurons was motivated by the idea that the output layer has one node per class label in the model.

3.3. Logistic Regression

A categorization approach called logistic regression [23] forecasts the potential occurrence of categorically dependent variables. In order for logistic regression to work, all of the dependent variables must have a binary character. An activation function is also utilized in logistic regression to compute the loss function and estimate the weights' values. The intended result is obtained after the loss function is minimized.

4. RESULTS AND DISCUSSION

One of the primary factors used to determine which model is superior to the others is accuracy of the models. Using the sklearn library's Accuracy Score and Cross-Validation methods, we determined the model's accuracy.

Table 3. Accuracy of Models

	Model	Train Score	Testing score
1	Neural Network	81%	74%
2	Gradient boosting	78%	73%
3	Logistic Regression	70%	7%

Accuracy score:
The set of labels predicted by the models must perfectly match that of the expected output in order for the accuracy score to be calculated.

Where n samples is the total number of predictions produced, yi prediction and y is the desired output. The formula below can also be used to compute it:

$$Accuracy\ Score = \frac{TP+TN}{TP+TN+fp+fn}$$

Where TN = True Negatives, TP = True Positives, fn = False Negatives and fp = False Positives.

4.1. PREDICTION ON WEB APPLICATION

In this part, we will show the steps of the utilization of our web application. In other to make a prediction, we need to run the Flask server and the frontend application then, fill up all the inputs and submit. Figure 6 shows a prediction example.

Figure 6. Prediction sample

5. CONCLUSION

Every individual should be concerned about the rising number of deaths from heart disease. As a result of the growing population, hospitals are less effective in providing prompt care. Because of this, a quick fix is required. Logistic Regression, Gradient boosting, ANN, and other machine learning models were utilized. When a patient has a heart condition, it is possible to tell. We produced synthetic data to lessen the over-fitting of the models. To increase the effectiveness of our model, we thoroughly examined the dataset, cleansed the data, and created a brand-new feature, BMI.

In terms of the test score, or 74%, the ANN performs best. In the future, we can use a multiple feature selection technique to extract the best features, build models, and create applications using real-time hospital data that will aid clinicians in identifying cardiac problems.

REFERENCES

[1]   World Health Organization. Joint WHO/FAO Expert Consultation on Diet, Nutrition and the Prevention of Chronic Diseases. 2002. Report No. 916.

[2]   Heart rate variability in critical illness and critical care Buchman, Timothy G. MD, PhD*; Stein, Phyllis K.PhD*; Goldstein, Brahm MD†

[3]   J. Thomas and R. T. Princy, "Human heart disease prediction system using data mining techniques," 2016 International Conference on Circuit, Power and Computing Technologies (ICCPCT), 2016, pp. 1-5, doi: 10.1109/ICCPCT.2016.7530265.

[4]   Liang, H., Tsui, K. L., Ni, H., & Zhu, Y. (2020). Cardiovascular disease detection using deep learning: a review. Frontiers in physiology, 11, 1161. doi: 10.3389/fphys.2020.01161.

[5]   Attia, Z., Khandoker, A. H., Khalaf, K., & Jamil, M. (2019). Automated detection of cardiovascular disease using deep learning techniques. Journal of medical systems, 43(8), 233. doi: 10.1007/s10916-019-1387-

[6]   Gupta, A., Shukla, A., & Srivastava, S. (2020). Cardiovascular disease prediction using deep learning algorithm. International Journal of Advanced Science and Technology, 29(3), 4752-4759. doi: 10.14257/ijast.2020.29.03.427.

[7] Singh, P., Kumar, P., & Sharma, A. (2021). Deep learning-based detection of cardiac arrest using ECG signals. Health information science and systems, 9(1), 1-11. doi: 10.1007/s13755-021-00134-7.

[8] Xue, J., Huang, C., Cui, W., & Yang, S. (2019). Machine learning for cardiovascular disease detection and diagnosis. Journal of healthcare engineering, 2019, 7941412. doi: 10.1155/2019/7941412.

[9] Kamath, M. V., Wadhera, R. K., & Rogers, J. G. (2017). Biomarkers in cardiovascular disease: prospects for personalized diagnosis and treatment. Current cardiology reports, 19(12), 129. doi: 10.1007/s11886-017-0912-6.

[10] White, S. K., Prasad, S. K., & Plein, S. (2019). Cardiac magnetic resonance imaging in the detection of cardiovascular disease. The Lancet, 393(10175), 323-335. doi: 10.1016/S0140-6736(18)32570-7.

[11] Wang, Y., Min, J. K., Khuri, J., Xue, H., & Xie, B. (2019). Mobile health applications for the detection and management of cardiovascular disease. Journal of the American College of Cardiology, 74(10), 1162-1176. doi: 10.1016/j.jacc.2019.06.046.

[12] Khan, M. S., Ullah, I., Riaz, M., Fazal, I., Khan, S., & Alharbi, N. S. (2021). Early detection of cardiovascular disease using machine learning techniques on electronic health records: a systematic review. fhjpmtHealthcare, 9(1), 38. doi: 10.3390/healthcare9010038.

[13] Ke, G., Meng, Q., Finley, T., Wang, T., Chen, W., Ma, W., ... Liu, T. Y. (2017). LightGBM: A Highly Efficient Gradient Boosting Decision Tree. In Advances in Neural Information Processing Systems (pp. 3146-3154).

[14] Yegnanarayana, B. (2009). Artificial neural networks. PHI Learning Pvt. [2] Azzopardi, L., "Cognitive Biases in Search: A review and reflection of cognitive biases in Information Retrieval," In Proceedings of the 2021 ACM SIGIR Conference on Human Information Interaction and Retrieval (CHIIR '21), 2021.

Thermophysical Behavior of the Treated Date Palm Tree Leaf- Reinforced Polyvinylchloride/Styrene Acrylonitrile Copolymer/Low-Density Polyethylene Ternary Composite

Samira Maou[1,4,*], Yazid Meftah[1,3], Antoine Kervoelenc[2],
Ahmed Meghezzi[1] Yves Grohens[2]

[1]*Laboratoire de Chimie Appliquée, Université Mohamed-Kheider de Biskra, Biskra 07000, Algeria, s.maou@univ-biskra.dz.,ORCID:0000-0002-8309-5441*

[2]*IRDL, CNRS, Centre de Recherche Christian Huygens, Rue de Saint-Maudé, 56100 Lorient, France.*

[3]*Ecole Normale Supérieure de Boussaada, Boussaada 28201, Algeria.*

[4]*IRDL, CNRS, Centre de Recherche Christian Huygens, Rue de Saint-Maudé, 56100 Lorient, France.*

[5]*Département de Chimie, Université Hassiba Ben Bouali de Chlef, Chlef 02180, Algeria.*

ABSTRACT

Date palm tree leaf-reinforced polymer composites are advantageous in terms of being sustainable and low-cost. In the present study, ternary composites of polyvinylchloride (PVC) reinforced with treated date palm tree leaves (TDPL) (10, 20, and 30 wt.%), styrene acrylonitrile (SAN) copolymer, low-density polyethylene (LDPE) were fabricated (PVC/SAN/LDPE) using an extrusion process. TDPL and SAN copolymer were used to improve the interfacial bonding, compatibility, and thermomechanical properties of the composite. Morphological behavioral analysis revealed that the incorporation of SAN copolymer enhanced the compatibility of the blend. Mechanical studies revealed improved tensile strength and hardness of the PVC/SAN/LDPE composite. In addition, the flexural and tensile modulus of the composite increased with increasing date palm leaves (DPL) content. Thermal analysis revealed increased Tid and Tmax, indicating improved thermal stability of the composite. Moreover, scanning electron microscopy revealed that the ternary PVC/LDPE blend modified with SAN copolymer and 30 wt% TDPL exhibited enhanced interfacial adhesive bonding compared with the binary PVC/LDPE blend; this improvement was also supported by the results of thermogravimetric and mechanical behavioral analyses.

Keywords: *Polyvinylchloride (PVC), Styrene acrylonitrile (SAN), Treated date palm tree leaves (TDPL), Mechanical behavioral analyses*

1. INTRODUCTION

Over the past few decades, fibers derived from plants, such as date palm [1], jute [2], and Aloe-vera [3], have garnered much research attention owing to their various economical, technical, and environmental benefits [4]. Natural fibers play important roles in quotidian life, with several uses in the construction sector [5]. Date palm tree leaves (DPL) represent a renewable, a nonabrasive, and an abundant source in not only the Algerian oasis agriculture but also all Saharan countries in northern Africa [6]. These natural fibers have low specific weight and cost yet show comparable strength and hardness to synthetic fibers, offering excellent mechanical characteristics [7]. Indeed, this natural resource can be turned into a value-added product through the manufacture of composites with various plastic materials. As such, DPL may be an interesting and eco-friendly alternative for use as a synthetic filler or reinforcement in advanced composites [8].Various plastic materials in the form of waste at landfill sites lead to environmental pollution [9]. Recycling is one of the simplest approaches to minimize pollution [10]. However, the behavior and properties of the recycled materials are poor, due to low compatibility and adhesion among various plastic materials [11]. Specifically, immiscible polymer blends often exhibit inferior thermal and mechanical properties to neat polymers [12]. Melt blending is one of the most frequently used processes for mixing plastic materials that contain a percentage of polyethylene (PE), polypropylene (PP), polystyrene (PS), and polyvinylchloride (PVC) [13–15].

A remarkable strategy to overcome the drawbacks of compatibility and adhesion is the introduction of small quantities of a third component used as a compatibilization agent, which serves as the bridge linking the polymer–polymer interfaces for blend compatibilization, and/or bio-reinforcement to the polymer matrix [16,17], which may markedly alter the mechanical characteristics of the polymer blends. In this regard, styrene acrylonitrile copolymer (SAN), polyethylene-graft-maleic anhydride (PE-g-MAH) [18] and styrene-ethylene-butylene-styrene-graft-maleic anhydride (SEBS-g-MA) [19] have been used to improve the interfacial compatibility of polymer blends and composite systems [20].

Recently, green composites have attracted much attention and have found numerous applications, thanks to their improved mechanical, morphological,

and thermal properties [21]. To fabricate good green composites, it is important to enhance the bonding adhesion among plastic polymer blends and natural fibers [22]. Another important strategy for improving the behavior of green composites is to enhance the compatibility between the natural reinforcement and polymer matrices. Alkaline modification has been frequently applied to enhance the interfacial bonding as well as the bonding between the matrix and fibers by reducing non-cellulosic parts, leading to the significant improvement of fiber surface [23]. To this end, the objective of the present study was to fabricate a green composite using PVC reinforced with untreated or treated DPL, SAN copolymer, and low-density polyethylene (LDPE) via melt blending extrusion. Furthermore, different behaviors of the fabricated green composites were investigated.

2. EXPERIMENTAL

Raw materials

LDPE pellets (melting point = 129°C, the specific enthalpy of melting = 106 J/g) and PVC 4000 M with a K value 67- 72, and Bis (2-ethylhexyl) terephthalate (DOP) were supplied by the "National Petrochemical Company (ENIP)" in Skikda, Algeria. Ca/Zn stearate was purchased from Nanjing OMYA Fine Chemical Ind. Co. Ltd. (Nanjing China). SAN copolymer with acrylonitrile (AN) content of 32 wt.%, sodium hydroxide (NaOH) and acetic acid (CH3COOH), were purchased from Sigma Aldrich, France. Date palm tree leaves, were collected from the local Sidi-Okba oasis of southern Algeria.

Preparation of DPL samples

Extraction procedure of the DPL: In this study, the collected DPL were immersed into a big glass beaker filled with deionized water at 75 °C for 2 h to remove the dust, wax and impurities. DPL were dried by sunshine in 5 days. These dried DPL were crushed by a coffee blender and sieved into different particle sizes (<1mm).

Alkali modification of the DPL: Pre-treatment was conducted by soaking the DPL in a 2L glass beaker filled with NaOH solution (5 %. wt.) for 1 h at 80°C. Finally, the sample was fully washed with deionized water and then neutralized with the acetic acid solution. The TDPL were then filtered and dried at 60 ° C for 2 days.

Preparation of the DPTL/PVC/SAN/LDPE composites

The PVC with (5%. wt. of Ca/Zn and 20%. wt of DOP), SAN and LDPE were added slowly at the same time in a laboratory twin screw extruder, with a processing temperature ranging from 165°C and a speed of 60 rpm. The temperature of the melt blending was increased to 170° C to make a homogenous blend. Dried DPTL was added slowly to this polymer blend during melt mixing. The composite sample was cooled to room temperature and ground using Grind Machine. The composite samples were obtained using the compression molding press at 170° C under a pressure of 200 bar for 5 min. The sample code and designation of the composites are presented in Table 1.

Table 1. The sample code and designation of the blends and composites

Sample code	Designation				
	PVC	SAN	LDPE	DPL (phr)	
	(phr)	(phr)	(phr)	Untreated	Treated
BC0	20	-	80	-	-
BC1	20	10	80	-	-
BC2	20	10	80	10	
BC3	20	10	80		10
BC4	20	10	80	30	-
BC5	20	10	80	-	30

3. CHARACTERIZATION

Morphological properties: Fracture Surfaces of the blend and composites were prepared by liquid nitrogen freezing before being manually broken down., thin gold coating. Images were recorded with an SEM, model JEOL JSM-6031.

Thermogravimetric analysis (TGA): Thermal decomposition of the blend and composites were performed on a thermogravimetric analyzer (TGA/ DSC STARE, Mettler Toledo/ TA Instruments) in the temperature range of 20 to 600°C at 10 °C/min heating rate under nitrogen atmosphere.

Mechanical tests: Tensile and flexural behaviors of the blend and composites were measured using an MTS Synergy RT1000 machine under ambient conditions. Tensile samples were tested according to ISO: 527-2 at a crosshead speed of 3 mm/min. Three-point flexural samples were conducted according to ISO:14125 at a crosshead displacement speed of 1.5 mm/min. At least five samples were tested for each formulation.

4. RESULTS AND DISCUSSION

Morphology of the PVC/SAN/LDPE composite: Figure 1 illustrates the fracture surface microtopography of the blends and composites containing 10 and 30 wt.% DPL at low and high magnifications. The voids in the BC1 blend matrix and BC2 composite can be observed in Figure 1. The interface between the raw DPL fibers and the PVC/SAN/LDPE blend matrix was poorly bonded, and the raw DPL fibers did not adhere to the PVC/SAN/LDPE blend matrix due to numerous impurities distributed on the DPL surface, in addition to the formation of lignin and wax layers. Moreover, there were no large interfacial gaps and voids in the BC3 and BC5 sections, indicating that the alkaline treatment of DPL could strengthen the interfacial bonding in the composite system, potentially improving its mechanical properties Bessa et al [24]. This improvement of compatibility resulted from the reduction of hemicellulose and lignin content due to alkalization. Meanwhile, the compact structure also prevented the dispersion of water molecules and reduced water uptake of the composites.
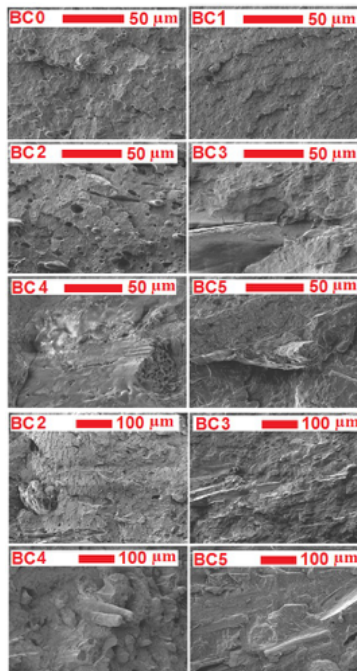

Figure 1. SEM micrographs of the PVC/SAN/LDPE blend and composites.

Thermal properties of the PVC/SAN/LDPE composite:

The blends and composites showed similar thermal degradation patterns (see Figure 2a-b); as such, thermal decomposition occurred in two stages between 239°C and 299°C for the former and between 300.05°C and 500°C for the latter. The values of the first decomposition temperature (T5%); decomposition temperatures for 10%, 20%, and 50% weight loss; and decomposition temperature for the maximum weight loss (Tmax) obtained from the derivative thermogravimetric curves are presented in Table 2. The BC0 blend underwent thermal degradation at the T5% value of 279°C, and the BC1, BC3, and BC5 composites and the DPL fibers underwent thermal degradation at the T5% values of 298°C, 291°C, 273°C, and 243°C, respectively. The introduction of SAN polymer into the PVC/LDPE blend did not alter the decomposition pattern but significantly enhanced the thermal stability and increased Tmax toward the highest value for thew blend matrix. Therefore, SAN copolymer altered the maximum weight loss decomposition behavior and improved the thermal stability of the PVC/LDPE blend.

The TGA curve of the TDPL showed an initial weight loss between 50 and 110 °C associated with the removal of water and all almost primary volatile components. The degradation of alkali modified DPL showed only one step at about 310 °C which corresponded to cellulose and hemicellulose degradation since most of the lignin and residues were removed after alkaline modification. Comparing the BC3, BC5 composites with the B0 blend matrix, indicated that the composite underwent faster thermal degradation because of the presence of the fiber effect which composes the cellulose, hemicellulose, and lignin, and these latter compositions degrade over a wide range of different temperatures compared to the blend matrix. The char yield is directly related to the potential flame retardation in polymers. This latter indicates that an increase of the lignocellulosic filler content can reduce the formation of combustible gases, lowering the thermal degradation exotherm and so hindering the thermal conductivity of the combustion processes. Similar observations were reported by Bessa et al. [24].
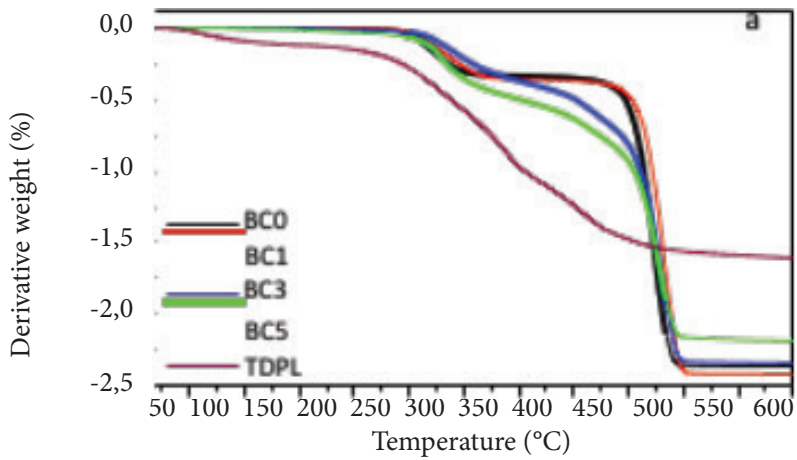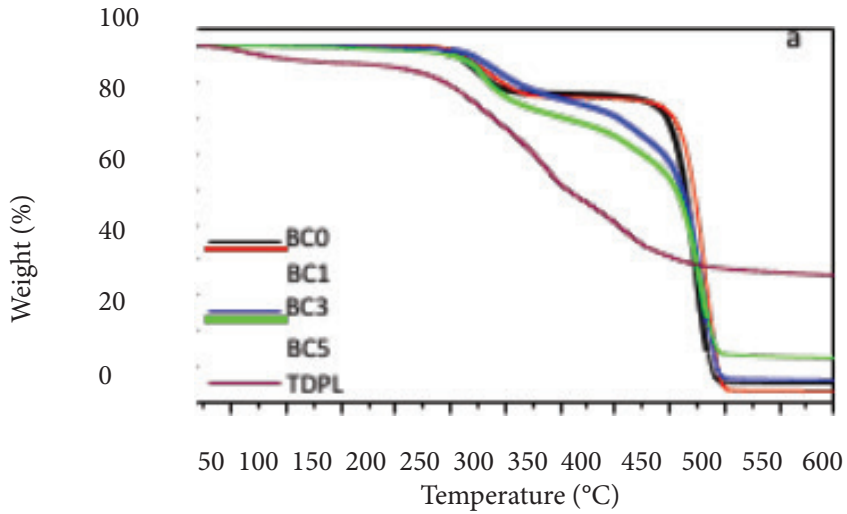
**Table 2.** The decomposition temperature of the blends and composites

Sample	T5% (°C)	T10% (°C)	T20% (°C)	T50% (°C)	Residue left (%)
BC0	244.84	284.76	449.12	467.77	3.88
BC1	253.26	298.91	454.84	477.54	3.23
BC3	264.53	310.22	403.28	471.65	6.57
BC5	261.05	286.98	348.16	469.57	12.92
TDPL	239.12	241.67	287.17	403.13	36.25

Mechanical properties of the PVC/SAN/LDPE composite: The tensile and flexural, hardness and elongation at break properties of the blends and composites containing 10wt.% and 30 wt.% DPL fibers are plotted in Figures (3-5). Alkaline modification can effectively improve the mechanical performance of the composites, especially the tensile and flexural modulus. Compared with the BC0 blend, the tensile and flexural strength of the BC1 blend were increased by 25.80 % and 9.89 %, respectively. The results show the influence of the SAN on the mechanical behaviors of the PVC/LDPE blend. The incorporation of the SAN into the PVC/LDPE blend promotes the phase dispersion of the PVC and LDPE and also improves the interfacial bonding. As a result, the SAN copolymer used here is compatible with PVC. A similar behaviors were also observed by Xu et al [25].
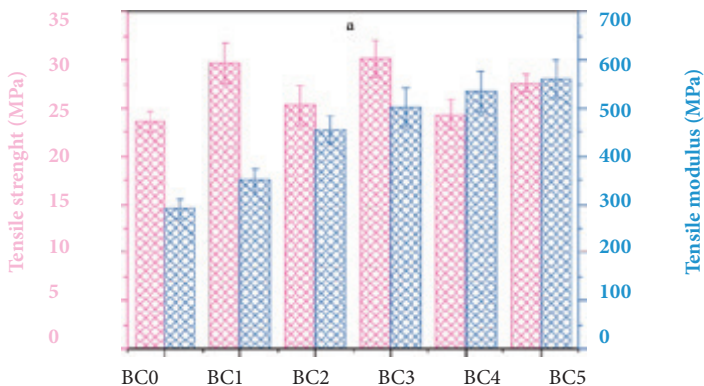

Figure 3. Tensile properties of the PVC/SAN/LDPE composites.

Samira Maou, Yazid Meftah, Antoine Kervoelenc, Ahmed Meghezzi, Yves Grohens

Figure 3 indicates that the alkali treatment has a greater influence on the tensile modulus of the TDPL than the raw DPL reinforced composite. The tensile modulus of the BC3(501.65 MPa) and BC5(560.24 MPa) composites are significantly different from that of BC2 (456.36 MPa) and BC4 (534.65 MPa), indicating that the use of the alkali treatment can effectively improve the interfacial bonding between the DPL fiber and the PVC/SAN/LDPE matrix. When the fiber loading was 30 wt.%, the tensile modulus of sample BC4 and Sample BC5 were 534.65 MPa and 560.24 MPa, respectively that of PVC/SAN/LDPE blend.Compared with the BC1 blend matrix in figure 4, the flexural modulus of the BC2, BC3, BC4, and BC5 were increased by 32.71%, 37.03%, and 64.30.5%, and 84.64 %, respectively. This result revealed that the SAN copolymer and TDPL strengthened the intermolecular interactions, thus increasing the hardness of the PVC/SAN/LDPE composite through crosslinking. The effect of the DPL content on the flexural modulus of the composite is obvious. When the TDPL fibers were used as a reinforcement, their flexural properties were superior to those of the composite using raw DPL fibers. As a result, the SAN copolymer works as a compatibilizer of the PVC/LDPE blend, and alkali solution can be used as an alternative to various treatments, which can effectively improve the interface compatibility during the preparation of the composite material.
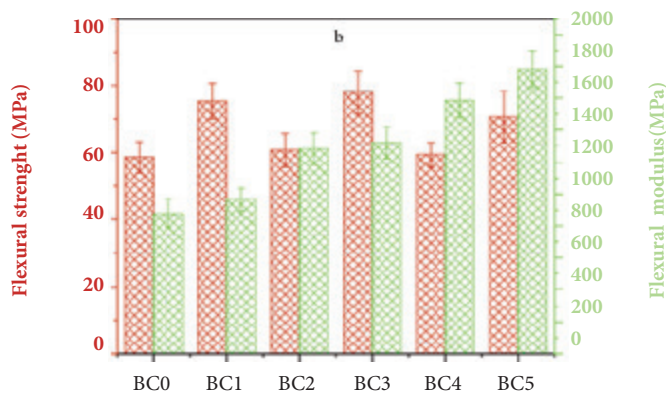
Figure 4. Flexural properties of the PVC/SAN/LDPE composites.

The hardness increases with an increase in TDPL content up to 30wt.% but decreases slightly in raw DPL reinforced composites at10 wt.%, 20 wt.%, and 30wt.%. The increase in raw DPL creates complications in its suitable blending. As shown in figure 5, a significant decrease of the elongation at break was observed with increasing DPL fibers concentration. The agglomeration of raw DPL fibers at higher loading leads to irregular agglomerate dispersions in the blend [23], which results in a decrease in surface resistance to the penetration. This latter affects the hardness and elongation at break results of the PVC/SAN/LDPE composites.
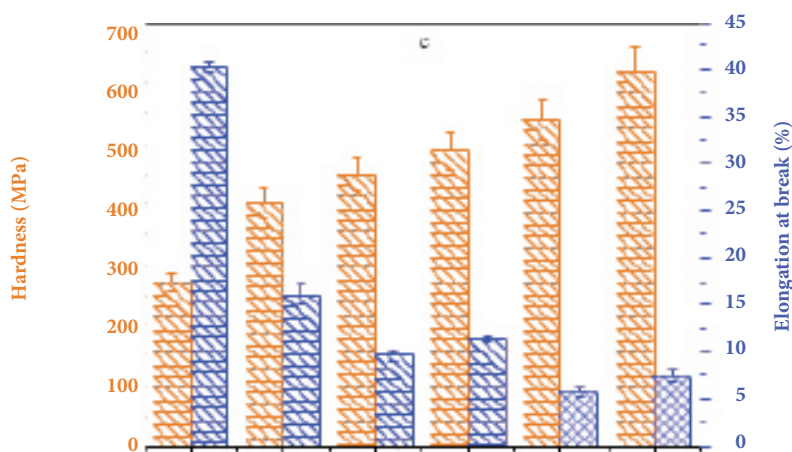
Figure 5. Hardness and elongation at break of the PVC/SAN/LDPE composites.

5. CONCLUSION

In the present work, the PVC/SAN/LDPE blend, DPL fibers reinforced composites were prepared. The results indicate that the addition of the SAN copolymer as a compatibilizer enhanced the thermophysical behaviors of the PVC/LDPE blend. The SAN copolymer helps the formation of chemical bonds between PVC and LDPE polymer, and the TDPL fibers enhanced the interfacial compatibility between the DPL and PVC/SAN/LDPE blend matrix. As a type of compatibility agent, the TDPL fibers and SAN copolymer provided a synergistic effect for preparing environmentally friendly PVC/SAN/LDPE composite with excellent thermophysical behavior.

Samira Maou, Yazid Meftah, Antoine Kervoelenc, Ahmed Meghezzi, Yves Grohens

ACKNOWLEDGEMENTS

REFERENCES

[1] Awad S, Zhou Y, Katsou E, Li Y, Fan M. A Critical Review on Date Palm Tree (Phoenix dactylifera L.) Fibres and Their Uses in Bio-composites. Springer Netherlands; 2020. https://doi.org/10.1007/s12649-020-01105-2.

[2] De Fátima V. Marques M, Melo RP, Da S. Araujo R, Do N. Lunz J, De O. Aguiar V. Improvement of mechanical properties of natural fiber-polypropylene composites using successive alkaline treatments. J Appl Polym Sci 2015;132:1–12. https://doi.org/10.1002/app.41710.

[3] Dehouche N, Idres C, Kaci M, Zembouai I, Bruzaud S. Effects of various surface treatments on Aloe Vera fibers used as reinforcement in poly(3-hydroxybutyrate-co-3-hydroxyhexanoate) (PHBHHx) biocomposites. Polym Degrad Stab 2020;175:109131. https://doi.org/10.1016/j.polymdegradstab.2020.109131.

[4] Chaudhary V, Ahmad F. A review on plant fiber reinforced thermoset polymers for structural and frictional composites. Polym Test 2020;91:106792. https://doi.org/10.1016/j.polymertesting.2020.106792.

[5] Masri T, Ounis H, Sedira L, Kaci A, Benchabane A. Characterization of new composite material based on date palm leaflets and expanded polystyrene wastes. Constr Build Mater 2018;164:410–418. https://doi.org/10.1016/j.conbuildmat.2017.12.197.

[6] Meftah Y, Tayefi M, Fellouh F, Maou S, Meghezzi A. Influence of Alkali Treatment and Dune Sand Content on the Properties of Date Palm Fiber Reinforced Unsaturated Polyester Hybrid Composites. Rev des Compos des matériaux avancés 2020;30:161–167. https://doi.org/10.18280/rcma.303-406.

analysis. Compos Part A Appl Sci Manuf 2017;103:292–303. https://doi.
org/10.1016/j.compositesa.2017.10.017.

[8]   Gupta MK, Srivastava RK. Mechanical Properties of Hybrid
Fibers-Reinforced Polymer Composite: A Review. Polym - Plast Technol
Eng 2016;55:626–642. https://doi.org/10.1080/03602559.2015.1098694.

[9]   Liu Y, Zhou C, Li F, Liu H, Yang J. Stocks and flows of polyvinyl
chloride (PVC) in China: 1980-2050. Resour. Conserv. Recycl 2020;154.
https://doi.org/10.1016/j.resconrec.2019.104584.

[10]   Saxena D, Maiti P. Utilization of ABS from plastic waste through
single-step reactive extrusion of LDPE/ABS blends of   improved
properties.   Polymer   (Guildf)   2021;221:123626. https://
doi.org/10.1016/j.polymer.2021.123626.

[11]   Maciel AV, Machado JC, Pasa VMD. The effect of temperature
on the properties of the NBR/PVC blend exposed to ethanol fuel and
different gasolines. Fuel 2013;113:679–89. https://doi.org/10.1016/j.
fuel.2013.05.101.

[12]   Cheng J, Yang X, Dong L, Yuan Z, Wang W, , Wu S, Chen S,
Zheng G, Zheng W, Zheng D, Wang H. Effective nondestructive eval-
uations on UHMWPE/Recycled-PA6 blends using FTIR imaging and
dynamic mechanical analysis. Polym Test 2017;59:371–376. https://doi.
org/10.1016/j.polymertesting.2017.02.021.

[13]   Czégény Z, Jakab E, Blazsó M, Bhaskar T, Sakata Y. Thermal
decomposition of polymer mixtures of PVC, PET and ABS containing
brominated flame retardant: Formation of chlorinated and brominated
organic compounds. J Anal Appl Pyrolysis 2012;96:69–77. https://doi.
org/10.1016/j.jaap.2012.03.006.

[14]   Wu J, Chen T, Luo X, Han D, Wang Z, Wu J. TG/FTIR anal-
ysis on co-pyrolysis behavior of PE, PVC and PS. Waste Manag
2014;34:676–82. https://doi.org/10.1016/j.wasman.2013.12.005.

[15]   Maou S, Meghezzi A, Nebbache N, Meftah Y. Mechanical, morphological, and thermal properties of poly(vinyl chloride)/low-density polyethylene composites filled with date palm leaf fiber. J Vinyl Addit Technol 2019;25: E88-E93. https://doi.org/10.1002/vnl.21687.

[16]   Jiang L, He C, Fu J, Xu D. Enhancement of wear and corrosion resistance of polyvinyl chloride/sorghum straw-based composites in cyclic sea water and acid rain conditions. Constr Build Mater 2019;223:133–141. https://doi.org/10.1016/j.conbuildmat.2019.06.216.

[17]   Jin DOOW, Shon KHO, Kim BKYU, Jeong HANMO. Compatibility enhancement of ABS/PVC blends 1998;4628. https://doi.org/10.1002/(SICI)1097-4628(19981024)70.

[18]   Pereira LM, Corrêa AC, De Sá Moreira De Souza Filho M, De Freitas Rosa M, Ito EN. Rheological, morphological and mechanical characterization of recycled poly (ethylene terephthalate) blends and composites. Mater Res 2017;20:791–800. https://doi.org/10.1590/1980-5373-MR-2016-0870.

[19]   Dobrovszky K, Ronkay F. Effects of SEBS-g-MA on rheology, morphology and mechanical properties of PET/HDPE blends. Int Polym Process 2015;30:91–99. https://doi.org/10.3139/217.2970.

[20]   Song YM, Wang QW, Han GP, Wang HG, Gao H. Effects of two modification methods on the mechanical properties of wood flour/ recycled plastic blends composites: Addition of thermoplastic elastomer SEBS-g- MAH and in-situ grafting MAH. J For Res 2010;21:373–378. https://doi.org/10.1007/s11676-010-0084-1.

[21]   Chauhan V, Kärki T, Varis J. Review of natural fiber-reinforced engineering plastic composites, their applications in the transportation sector and processing techniques. J Thermoplast Compos Mater; 2019; 28:1- 41. https://doi.org/10.1177/0892705719889095.

[22]   Al-Otaibi MS, Alothman OY, Alrashed MM, Anis A, Naveen J, Jawaid M. Characterization of date palm fiber- reinforced different polypropylene matrices. Polymers. 2020;12. https://doi.org/10.3390/polym12030597.

[23]   Maou S, Meghezzi A, Grohens Y, Meftah Y, Kervoelen A, Magueresse A. Effect of various chemical modifications of date palm fibers (DPFs) on the thermo-physical properties of polyvinyl chloride (PVC) – high-density polyethylene (HDPE) composites. Ind Crop & Prod. 2021;171:113974. https://doi.org/10.1016/j.indcrop.2021.113974.

[24]   Bessa W, Trache D, Derradji M, Tarchoun AF. Morphological, thermal and mechanical properties of benzoxazine resin reinforced with alkali treated alfa fibers. Ind Crops & Prod. 2021;165:113423. https://doi.org/10.1016/j.indcrop.2021.113423.

[25]   Xu C, Fang Z, Zhong J. Study on compatibilization-crosslinking synergism in PVC/LDPE blends. Die Angew Makromol Chem. 1993;212:45–52. https://doi.org/10.1002/apmc.1993.052120105.

Atomistic Multiscale Modeling of SWCNT Reinforced Polymer Nanocomposites: Effects of Waviness, Volufraction and Interface Material

Debangshu Paul[1]

Department of Mechanical Engineering, Bangladesh University of Engineering and Technology, Dhaka-1000, Bangladesh, debangshu.paul@gmail.com, ORCID: 0000-0001-8986-7839

ABSTRACT

Carbon nanotube (CNT) is a multifunctional nanostructured material with exceptional mechanical, thermal and electrical properties and one of the strongest materials known to men. CNTs are frequently used as reinforcements in composites. However, process induced defects like vacancies and curvature in CNT are common. Such defects are known to have detrimental effects on the overall properties of the composites. In an approach to quantify the effects of CNT waviness on mechanical properties of CNTs and their composites, a multiscale analysis is performed. At the nanoscale analysis, an atomistic model of wavy single walled CNT (Armchair and Zigzag) is developed and the effect of waviness ratio and wavelength ratio on Elastic modulus is studied. Then a finite element model is developed where fibers are oriented in two different process-induced patterns, aligned and random orientation. In each case, elastic modulus and shear modulus are determined in both longitudinal and transverse directions and the variation of their values with the change of waviness ratio as well as volume fraction are studied by finite element method where the dilute strain concentration tensor is obtained directly from a finite element solution. It was observed that the Elastic modulus decreases with increasing waviness of CNT, but after a certain value of waviness ratio, the decreasing rate becomes insignificant. Additionally, the modulus of the CNT decreases with diameter, while having drastic change in the larger diameter region. Though composite reinforced with CNTs follow similar trend with the atomic model, it was observed that at higher waviness ratio, alignments of CNTs have less impact on the modulus of the composite. Furthermore, it was observed that the overall strength of the composite increases non-linearly with the increment of volume fraction,and as expected, interface material reinforces the mechanical properties of the composite.

Keywords: *CNT, SWCNT, Single Walled Carbon Nanotube, Advanced Material, Wavy CNT, Composite, Atomistic Modeling*

1. INTRODUCTION

The discovery of Carbon Nanotubes (CNTs) only a couple of decades ago [1] have opened up a new era of multifunctional nanostructured materials. CNTs are hollow cylindrical shells of carbon atoms laid in a honeycomb pattern. Their modulus values have been shown on the order of 1 TPa, with strength several times that of graphite fibers [2-5]. Despite the prohibitive cost of manufacturing, carbon nanotubes are already being used in a wide range of applications including airplane and vehicle components, in bulletproof clothing and electronics [6].

Properties of multi and single-walled nanotubes (MWNTs or SWNTs) have been studied using both experiments and modeling. Molecular dynamics (MD) and elastic continuum modeling approaches have been used to estimate the characteristics of CNTs. However, a wide scatter can be seen in experimental and simulation data for moduli of CNTs. For example, experiments conducted by Treacy et al. [7], using Transmission Electron Microscopy (TEM) to measure the Young's modulus of MWNTs, found a mean value of 1.8 TPa with a variation from 0.40 to 4.15 TPa; while similar experiments by Krishnam et al. [8] observed Young's modulus ranging from 0.90 to 1.70 TPa. Wang et al. [9] conducted bending tests on cantilevered tubes of CNTs using atomic force microscopy and estimated the Young's modulus of 1.28 TPa. Poncharal et al. [10] observed the static and dynamic mechanical deflections of cantilevered MWNTs, which is induced by an electric field, and reported a modulus of about 1.0 TPa for small- diameter tubes.

Among the numerical and theoretical studies, molecular modeling in particular, which is based on the force field and total potential energy for CNTs in a macroscopic sense has been used most extensively (Iijima et al. [11]; Gau et al. [12]; Zhou et al. [13]; Belytschko et al. [14]). However, the computational expense for convergence requirements in MD simulations limits the size of CNTs that can be studied by this technique.

The other approach is the continuum/finite element method (Zhang et al. [15, 16]; Jin and Yuan [17]; Li and Chou [18, 19]). Since a nanotube closely resembles a continuum solid beam or shell on macro-scale, it is reasonable to model the nanotube as a frame or shell-like structure. Using this approach, the mechanical properties of such a structure can be obtained by classical continuum mechanics or finite element method. However, due to the uncertainty of the CNT wall thickness for both of the above

modeling techniques, the obtained mechanical properties of SWNTs or MWNTs have scattered values; for example, the results of axial Young's modulus ranged from about 1.0 to 5.5 TPa can be found in the existing literature [20].

Carbon nanotubes are stronger than most conventional reinforcements [2-5]. Not surprisingly, CNTs have been incorporated into various bulk materials to enhance the properties of the parent materials. Significant improvements have been reported for nanotube-reinforced polymers with regard to mechanical, electrical and thermal properties [21-23]. Such composites take advantage of the extraordinary electrical and thermal conductivity of CNTs to create multifunctional composites with improved electrical and thermal properties [24].

Although at the beginning, CNTs were thought to be cylindrical shells that consisted of regular hexagonal arrays of carbon atoms, it is now widely accepted that defects and morphological variations are common. Researchers have only started to look at the effects of these structural variations on the properties of CNTs as well as their composites [25, 26].

Another feature characteristic of nanocomposites is that the embedded CNTs are not straight but rather have significant curvature or waviness that varies throughout the composite [27]. While it is reasonable to surmise that this waviness reduces the effectiveness of the CNT reinforcement of

the polymer, the degree to which this is the case is unclear. The goal of this work is to develop a micromechanics-based model that can be used to assess the effect of nanotube waviness on the properties of composites. In the studies of Fisher, Bradshaw, and Brinson [28, 29], the problem was simplified by modeling the wavy CNTs as infinitely long straight NTs; the effect of waviness was incorporated using a reduced effective nanotube modulus determined via finite element (FE) modeling. The wavy CNT was modeled by using a straight CNT with a reduced modulus to determine the dilute strain concentration tensor analytically via Eshelby's solution [30]. In this work, an alternate approach is used. The NT is modeled as single wavelength long sinusoidal fiber and the dilute strain concentration tensor is obtained directly from a finite element solution. This approximates the NT and the surrounding matrix as a continuum; once the NT and surrounding matrix are modeled as a continuum, the length scale of the NT is no longer material to the analysis. Thus, the model developed in this article applies equally well to larger inclusions such as graphite fibers. As such, in this article the term fiber is used interchangeably with the term nanotube when speaking of the reinforcement phase of the composite material.

In this study, a finite element model of SWNTs was developed and their modulus of elasticity (longitudinal and transverse direction) with variation of the diameter and waviness of the CNT were consequently estimated. The key concept of the modeling is that the carbon nanotube can be treated as a frame like structure, and the primary bonds between two nearest neighboring atoms can be simulated as beam elements.

After developing a model for straight CNT, an elastic modulus was estimated and the tube thickness was adjusted to get relevant value as done in the past studies. Then waviness was applied to the CNT and the values of elastic modulus were calculated for different waviness as well as different diameters of the CNT. These values were used in this study in the Composite model to estimate the modulus of elasticity and shear modulus (both in the longitudinal and transverse direction) and six finite element solutions were performed to determine the constants by which a transversely isotropic material can be described. The study was carried out for aligned CNTs and randomly orientated of the CNTs to observe the effect of random orientation of CNTs in the composite (Figure 1).The variation of elastic modulus with volume fraction was studied and compared with the modified rule of mixture [31].
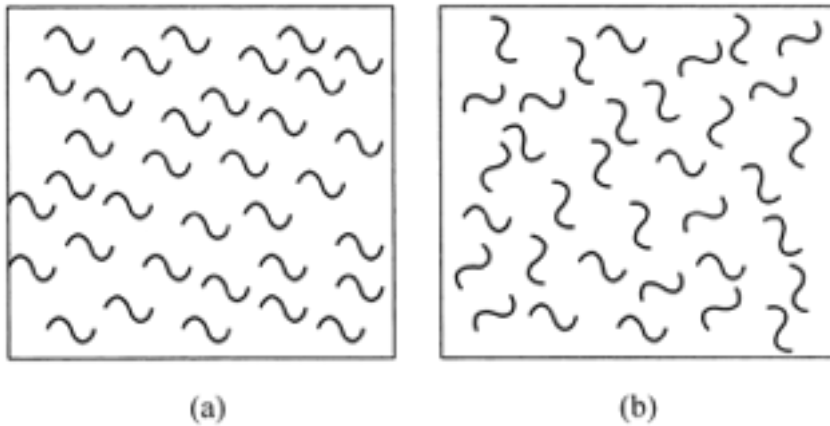
Figure 1. Wavy NT orientations: (a) similarly oriented wavy NTs with common axis directions and waviness planes; (b) wavy NTs randomly oriented in all directions with randomly oriented planes of waviness.

1.1. FE modeling

CNTs carbon atoms are bonded together with covalent bonds forming a hexagonal lattice. These bonds have a characteristic bond length αC-C and bond angle in the 3D space. The displacement of individual atoms under an external force is constrained by the bonds. Therefore, the total deformation of the nanotube is the result of the interactions between the bonds. By considering the bonds as connecting load-carrying elements, and the atoms as joints of the connecting elements, CNTs may be simulated as space-frame structures.

(i)   (ii)
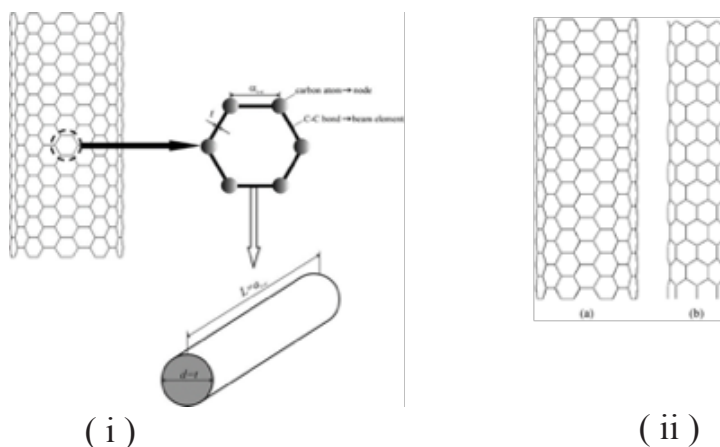
Figure 2. i) Schematic of a SWCNT as a space-frame structure.
ii) Side views of the FE meshes of the (a) (8,8) and (b) (8,0) SWCNTs. [32]

By treating CNTs as space-frame structures, their mechanical behavior can be analyzed using classical structural mechanics methods. Figure 2 depicts how the hexagon, which is the constitutional element of CNTs nanostructure, is simulated as structural element of a space- frame. In the same way, the entire nanotube lattice is simulated. The simulation leads to the correspondence of the bond length αC-C with the element length L as well as the wall thickness t with the element thickness. In the study, size of nanotube varied from zigzag (10,0) to (14,0) and armchair (6,6) to (10,10).

1.2. Elastic moduli of beam elements

According to classical structural mechanics, the strain energy of a uniform beam of length L and cross-section A under pure axial force N is,

$$U_A = \frac{1}{2}\int_0^L \frac{N^2}{EA}dL = \frac{1}{2}\frac{N^2 L}{EA} = \frac{1}{2}\frac{EA}{L}(\Delta L)^2$$

$$U_M = \frac{1}{2}\int_0^L \frac{M^2}{EA}dL = \frac{1}{2}\frac{EI}{L} = \frac{1}{2}\frac{EI}{L}(2\alpha)^2$$

Where ΔL = the axial stretching deformation. The strain energy of a uniform beam under pure bending moment M is,

Where α denotes the rotational angle at the ends of the beam. The strain energy of a uniform
beam under pure torsion T is,

Where, $\Delta\beta$ is the relative rotation between the ends of the beam and J the polar moment of inertia.

It can be concluded that $U_{c,\text{Æ}}$ represent the stretching energies in the two systems (molecular and structural), U_θ, U_M, the bending energies, and U_c, U_T the torsional energies. It can be assumed that the rotation angle 2α is equivalent to the total change $\Delta\theta$ of the bond angle, ΔL is equivalent to Δr, and $\Delta\beta$ is equivalent to $\Delta\varphi$. Therefore, by comparing Eqn. (3)–(5) with Eqn. (6)–(8), the following direct relationships between the structural mechanics parameters EA, EI and GJ and the molecular mechanics parameters k_r, k_θ and k_c are obtained,

Given the force constants , $k\theta$ and, kc the bond diameter and elastic moduli can be obtained from Eqn. (10).

Tserpes, K. and P. Papanikos [32] demonstrated a method for evaluating the diameter, elastic modulus and bulk modulus, and found the values to be d = 0.147, E = 5.49 TPa and G = 0.871 TPa. The procedure provides a unique value of bond diameter (= wall thickness). In order to compare the evaluated elastic moduli of the SWCNTs with the literature results, the FE model was implemented using various values of wall thickness and finally a fixed value of wall thickness (d = 0.13 nm) and *ac-c* = 0.1452 *nm* was used throughout the study.

1.3. Numerical Homogenization

The study used the mathematical model where the composite material is considered to have cylindrical fibers of infinite length, embedded in an elastic matrix. Because of the periodicity, the three dimensional representative volume element (RVE) can be used for FE analysis [33]. A transversely isotropic material is described by five constants. When the axis of symmetry is the fiber direction, 3D Hooke's law reduces to,

Once the components of the transversely isotropic tensor C are known, the five elastic properties of the homogenized material can be computed by Eqn. (13) – (17), i.e. the longitudinal and transversal Young's moduli E_1 and E_2, the longitudinal and transversal Poisson's ratios V_{12} and V_{23}, and the longitudinal shear modulus G_{12}, as follows,

2. COMPUTATIONAL METHOD

### 2.1. Elastic Modulus of Single-walled Carbon Nanotube

Polymer nanocomposites containing wavy CNTs were characterized in a two-step micromechanical approach. Firstly, individual CNTs were studied for effects of change of
waviness ratios ($^a/\lambda$) using an atomistic structure. The resulting nanostructure was studied in FEM and the complete 3D material constitutive matrix was populated by data generated through six different stress boundary conditions applied to the CNT.

2.2. Atomic modeling of Carbon nanotubes

The coordinates of carbon atoms in nanotubes of varying chirality were generated using a GNU code. These coordinates will be exported to commercial FE software using an in-house code that will generate the hexagonal lattice of the selected CNT and represent the lattice using link elements.
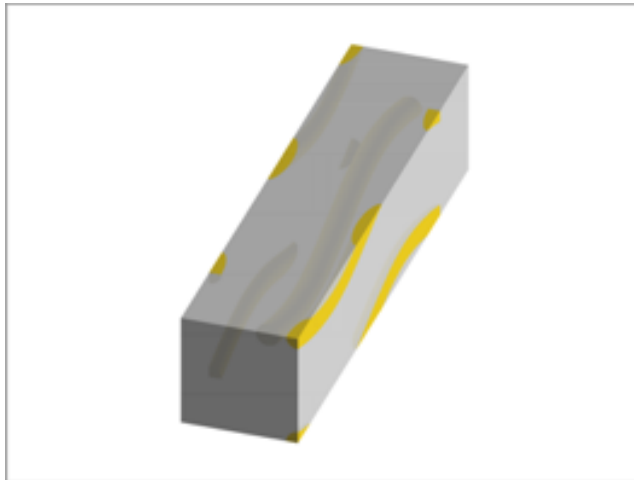
2.3. Carbon Nanotube

One end of the CNT was defined as fixed and force was applied at the other end. The value of displacement was collected from the horizontal parts of the CNT for calculating the average value of the strain. The horizontal part close to the application of the force shows negative displacement when the waviness increases, so values of displacement was taken at the horizontal part closest to the fixed end of the CNT (Figure 3 and Figure 4). Elastic modulus was calculated from the strain and stress determined from the applied force.
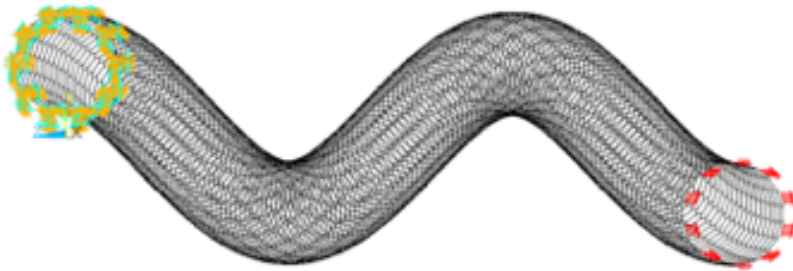
Figure 3. Atomic Structure of a (10, 10) CNT with boundary conditions at waviness ratio = 0.04 and Wavelength ratio =18.13

2.4. RVE of polymer composite reinforced with SWCNT

A continuum approach was utilized to model the wavy CNT as a curved solid beam in a representative volume element (RVE) of a polymer matrix (Figure 4). Consequently, the analysis at this macro-level incorporated the changes associated with CNT waviness, providing a more accurate prediction of the effective material properties of the nanocomposite. The polymer that was used for the composite matrix was Polystyrene with elastic modulus of 3.12 GPa. A volume fraction of 2.5% has been used in all the nanocomposites.

Figure 4. RVE of Composite reinforced with 2.5% aligned (14, 0) Carbon Nanotube at Waviness ratio = 0.024with the fiber direction

3. RESULT AND DISCUSSION

For each type of CNT Waviness ratio ( ) was varied from 0 to 0.08, where waviness of 0 stands for straight tube.

3.1. Elastic modulus of Single Walled armchair CNT with variation of Waviness

Three types of armchair CNTs ((6, 6), (8,8) and (10,10)) were studied and their moduli of elasticity were compared for same variation of waviness ratio (from straight tube to 8% waviness ratio). Waviness ratio is the ratio of amplitude to wavelength.

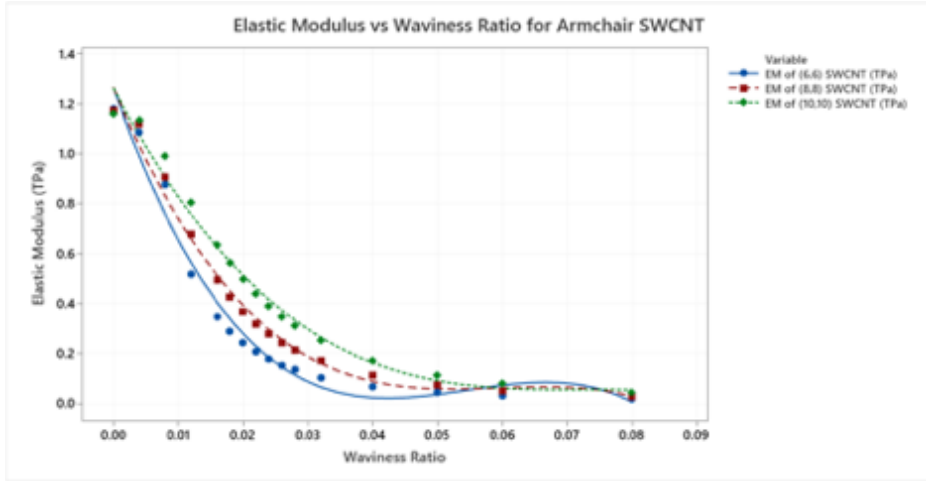## Elastic Modulus vs Waviness Ratio for Armchair SWCNT

Figure 5. Elastic modulus vs. Waviness Ratio of armchair carbon nanotube

Effect of waviness on elastic modulus of Single walled armchair Carbon Nanotube is illustrated in Figure 5. Elastic modulus decreases with increasing waviness. After a certain value of waviness ratio (approximately 0.04) the curve seems to be flattened and the decreasing rate of elastic modulus become insignificant. For a waviness ratio of 3.2%, elastic modulus decreases by around 85% of that of the straight nanotube.

3.2. Elastic modulus of Single Walled zigzag CNT with variation of Waviness

Three types of zigzag CNTs ((10, 0), (12, 0) and (14, 0)) were studied and their moduli of elasticity were compared for same variation of waviness ratio (from straight tube to 8% waviness ratio). Zigzag CNTs were chosen such that they have similar range of wavelength ratio as that of armchair CNTs.
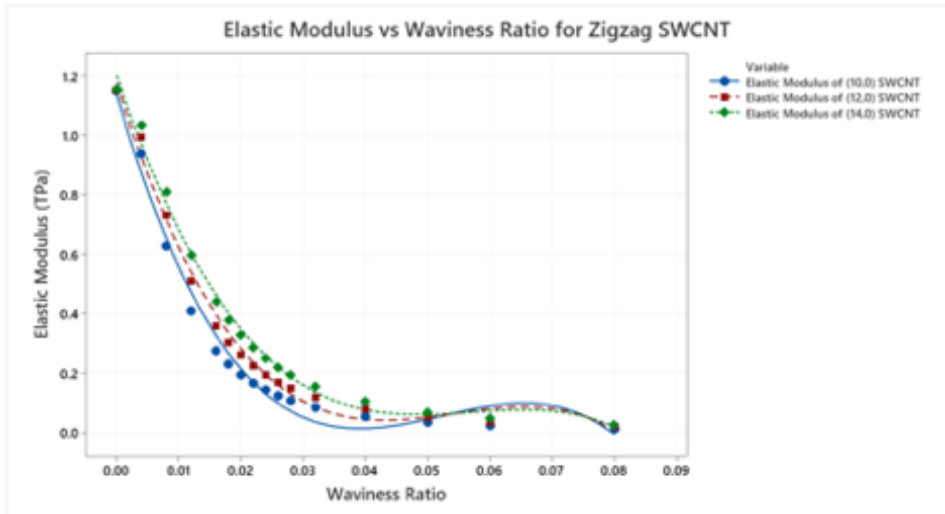
Figure 6. Elastic modulus vs. Waviness Ratio of zigzag carbon

Effect of waviness on elastic modulus of Single walled zigzag Carbon Nanotube is illustrated in Figure 6. Elastic modulus decreases with increasing waviness. After a certain value of waviness ratio (approximately 0.04) the curve seems to be flattened and the decreasing rate of elastic modulus becomes insignificant. For a waviness ratio of 3.2%, elastic modulus decreases by around 90% of that of the straight nanotube. The reduction in the values of elastic modulus is similar to the findings of Marino Brcic et al. [34] for straight CNTs. According to their study, in a (5, 5) CNT, longitudinal elastic modulus decreased by around 82.5% for an increment of waviness ratio of 3.5%.

It can be assumed that waviness imposes instability on the CNTs. As a result, with the increasing waviness it requires less stress to impose strain than that of a straight tube which is the most stable form. In the atomic scale, carbon atoms in the cusps of the wavy CNTs are deviated from the ideal location for optimum stiffness. Axial elongations tend to be favored by such CNTs, in order to achieve this optimum atomic distance, resulting in lower stiffness. The greater the wavelength ratio of a CNT, the greater the deviation of atomic positions from the optimum locations, and the easier it is for an atom to move relative to its closest neighbor. This explanation is found to be consistent with the sharp drop in stiffness of CNTs with high wavelength ratios. However, to explain this feature in the

FE analysis, where bond stiffness is independent of atomic distances, bond lines orientations are considered. Atomic bonds at the inner edge of a cusp are subjected to a greater amount of the axial load due to the alignment of such lines with the loading direction. While bond lines in the straight portions of the CNT, located in an inclined orientation due to the structure of the CNT, receive much lower portions of the boundary load component. As a result, only a small portion of the bonds, within the cusp zones in particular, support a major portion of the applied load in case of wavy CNTs, resulting in a lower overall stiffness for wavy CNTs.

Moreover, this effect is diminished beyond a wavelength ratio of approximately 0.4. Again, this is related to the atomic bonds within the cusp zones. Beyond a critical waviness ratio ($^a/\lambda$), atomic bond alignment change with increasing waviness becomes insignificant, so no change in stiffness can be observed beyond this critical wavelength ratio. This concept should be equally relevant for the atomic scale and the RVE.

3.3. Elastic modulus of Single Walled armchair CNT with variation of Diameter

In the current study, diameter has been represented by wavelength ratio, which is the ratio of wavelength to diameter ($^\lambda/d$). In the case of CNT, diameter changes with the change of indices (m, n). To study the effect of diameters of wavy CNTs on their modulus, armchair CNT from (6, 6) to (12, 12) were used with a resultant variation of diameter between 0.8193 nm to 1.6575 nm.

Elastic Modulus vs Wavelength Ratio for Armchair SWCNT
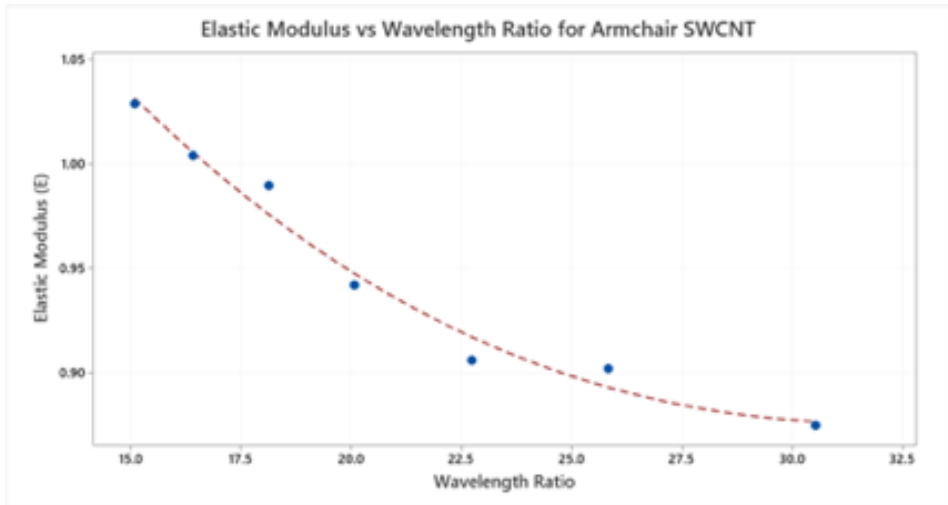
Figure 7. Variation of elastic modulus with varying diameter for (8, 8) CNTs with waviness ratio = 0.008

The change of diameter is represented by wavelength ratio, which is a dimensionless number and determined by the ratio of wavelength to diameter. In Figure 7, the elastic modulus decreases as the diameter of a Single walled armchair CNT is decreasing. Within the range of analysis, for a decrease in diameter by 50.57%, the modulus of elasticity decreases by 14.88%. It is also observed that CNT with higher wavelength ratio (ratio of wavelength to diameter; more the wavelength ratio smaller the tube diameter) has less strength than the CNT of lower wavelength ratio. Furthermore, the modulus of the CNT with lower wavelength ratio (larger diameter) decreases more drastically than that of higher wavelength ratio.

3.4. CNTs reinforced composites with aligned and random orientation:

For studying the composite, (8,8) armchair CNT and (14,0) zigzag CNT were selected as their diameters are almost same. This study considered two orientations: (1) aligned orientation and

(2) cross direction, which is the direction normal to the wave propagation represented the random orientation. The waviness of the CNTs cause them to be spaced apart which reduces the van der Waals forces and does not allow the CNTs to all be loaded at the same time, thus reducing the

strength of the composite. In the previous section it was explained how in FE analysis, CNT stiffness is reduced by the effect of waviness. In a similar fashion, the composite material with a wavy CNT exhibits reduced stiffness. It is to be noted that the scale of the analysis for an individual CNT was atomistic, while the composite analysis is conducted using the continuum approach. In the continuum analysis, it was assumed that the effect of CNT waviness was carried over from the atomistic simulation data, and interfacial interaction between the bulk matrix and a curved nanotube would further influence the overall stiffness of the composite.

3.5. Polymer composite reinforced with (8, 8) CNT

For (8, 8) CNT reinforced composite, a wavelength ratio = 22.73 and volume fraction = 2.5% were considered. From the simulation software, the values of the constants in stiffness matrix have been determined. Then Eqn. (12-17) were used to determine the values of elastic and shear modulus.
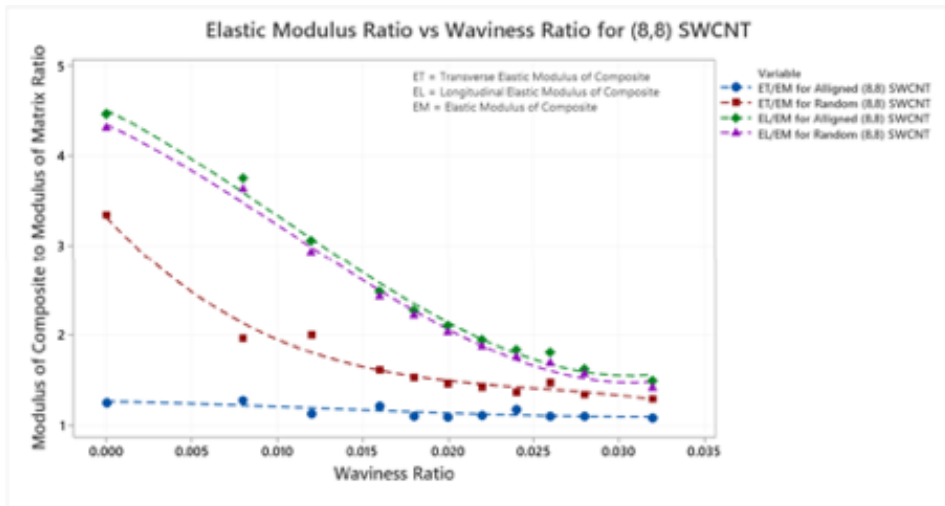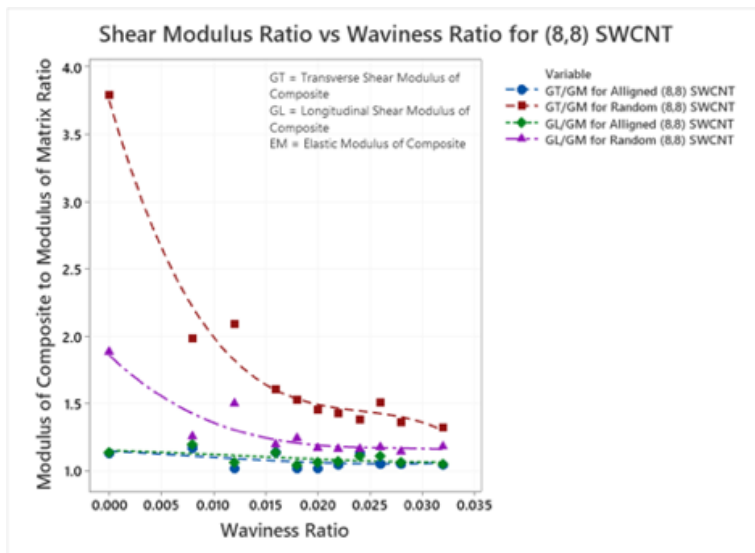

Figure 8. Elastic Modulus Ratio vs Waviness Ratio for (8,8) SWCNT with 2.5% volume fraction and wavelength ratio = 22.73

In Figure 3.4 variation of elastic modulus of nanocomposite reinforced with (8,8) CNTs with the increasing waviness ratio has been illustrated for both aligned and random orientations. The Elastic modulus of both orientations demonstrate downward trends with increasing waviness. The longitudinal elastic modulus (Figure 8) follows almost the same

trend as the (8, 8) CNT (Figure 5) and for aligned CNT, decreases by 66.7% as the waviness is increases to 3.2%. On the other hand, transverse elastic modulus (Figure 8) decreases with increasing waviness ratio in an irregular way and decreases by 13.6% as the waviness varies up to 3.2%. For random orientation, the longitudinal elastic modulus decreases by 67.2% as the waviness increases up to 3.2%, and decreases with a few fluctuating values to around 61.25%. Paunikar et al. also observed similar phenomenon in 2014 [35].

Composite with aligned orientation of CNT shows higher Longitudinal modulus than that of the random orientation, whereas the transverse elastic modulus increases significantly as the orientation is changed from aligned too random. Moreover, the variation due to alignment decreases with increasing waviness, which implies that at higher waviness ratio, alignments of CNTs have less impact on the modulus of the composite.

Figure 9. Shear Modulus Ratio vs Waviness Ratio for (8,8) SWCNT with 2.5% volume fraction and wavelength ratio = 22.73

Transverse shear modulus (Figure 9) decreases with increasing waviness ratio in an irregular way and decreases by maximum 10.1% as the waviness varies up to 3.2% for aligned orientation, whereas Longitudinal Shear Modulus decreases with increasing waviness ratio in an irregular way by 7.8%. For random orientation, Longitudinal shear modulus (Figure 9)
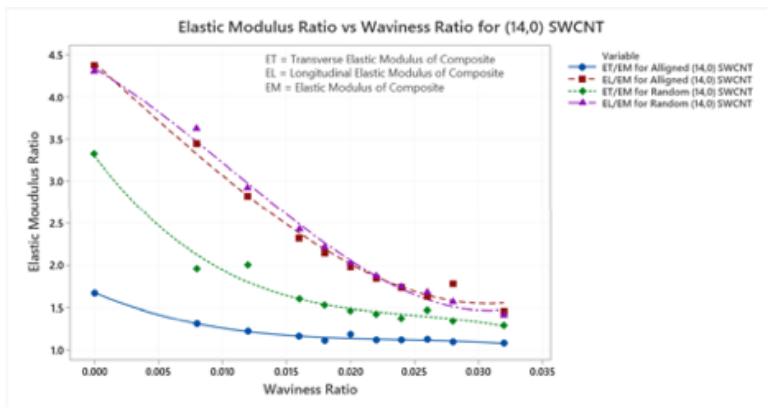
decreases with increasing waviness ratio in an irregular way and decreases by 40% as the waviness varies up to 3.2%, and the transverse shear modulus decreases with a few fluctuating values by 65.3%.

While the longitudinal elastic modulus has a smooth decreasing pattern, transverse elastic modulus and both types of shear modulus have fluctuating values with the variation of waviness. These effects are probably due to the non-uniformity caused by the waviness of the CNTs. The load is not distributed uniformly throughout the body in transverse direction. Hence, with increasing waviness, a wide scatter in data is observed.

Both longitudinal and transverse shear modulus increase significantly as the orientation is changed from aligned to random. Additionally, similar to the elastic modulus, the variation due to alignment decreases with increasing waviness, which implies that at higher waviness ratio, alignments of CNTs have less impact on the modulus of the composite.

3.6. Polymer composite reinforced with (14, 0) CNT

For (14, 0) aligned CNT reinforced composite, a wavelength ratio = 22.34 and volume fraction
= 2.5% were considered. From the simulation software, the values of the constants in stiffness matrix have been determined. Then Eqn. (13-18) were used to determine the values of elastic and shear modulus.

Figure 10. Elastic Modulus Ratio vs Waviness Ratio for (14,0) SWCNT with 2.5% volume fraction and wavelength ratio = 22.34

In Figure 10, variation of elastic modulus of nanocomposite reinforced with (14,0) CNTs with the increasing waviness ratio has been illustrated. For aligned orientation, the longitudinal elastic modulus decreases almost linearly and the value is reduced by maximum 66.8% for an increase in waviness up to 3.2%. Transverse elastic modulus decreases with some fluctuating values by maximum 35.4%. On the other hand, for random orientation, the longitudinal elastic modulus decreases almost linearly by around 68% as the waviness ratio is increased to 3.2%, whereas transverse elastic modulus decreases in a more irregular way by 49%.

Moreover, the longitudinal elastic modulus changes in a very small amount in comparison to transverse elastic modulus, but for this case (zigzag CNTs reinforced composite), the longitudinal elastic modulus for random-oriented is larger unlike that of armchair CNTs reinforced composite.
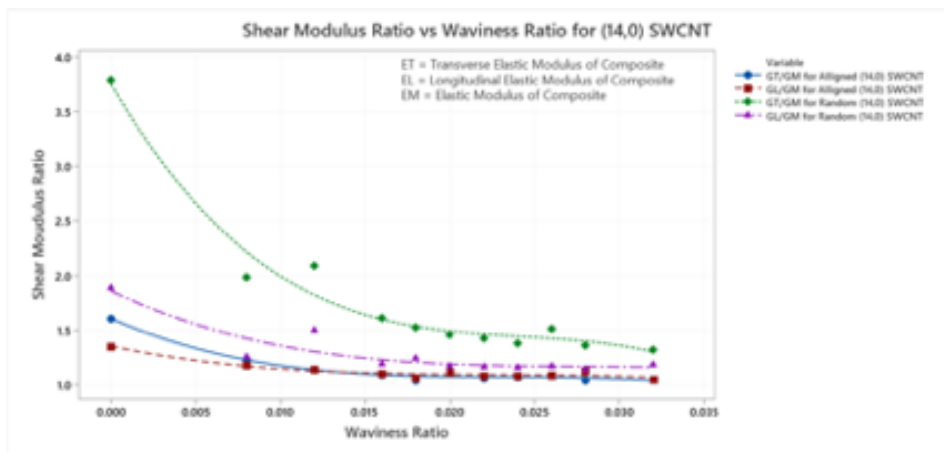
Figure 11. Shear Modulus Ratio vs Waviness Ratio for (14,0) SWCNT with 2.5% volume fraction and wavelength ratio = 22.34

Transverse shear modulus (Figure 11) and Longitudinal shear modulus decreases with increasing waviness ratio by maximum 35.3% and 22.4% as the waviness varies up to 3.2% for aligned orientation of CNTs.

On the other hand. Transverse shear modulus decreases with increasing waviness ratio with a few fluctuating values and decreases by 23.8% as the waviness varies up to 3.2%, whereas Longitudinal shear modulus decreases by 51.3%

3.7. Variation of Mechanical Properties in Nanocomposite with the change in volume fraction:

Polymer composite reinforced with aligned (8, 8) CNT
For (8,8) aligned CNT, at waviness ratio = 0.012, wavelength ratio = 22.73, elastic modulus of CNT = 0.68TPa: Volume fraction was varied from 0.5% to 10%. From the simulation software, the values of the constants in stiffness matrix have been determined.
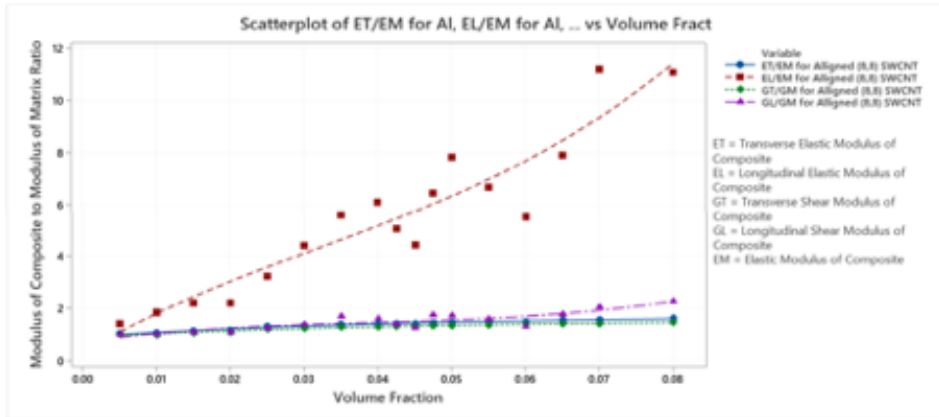

Figure 12. Modulus Ratio vs Waviness Ratio for (8,8) SWCNT with Waviness ratio = 0.012 and wavelength ratio = 22.73

In Figure 12, variation of elastic modulus of nanocomposite reinforced with aligned (8, 8) CNTs with the increasing volume fraction has been illustrated. Change of the longitudinal elastic modulus with increasing volume fraction found in the study have lower rate of increment than the values determined from modified rule of mixture [31]. There are fluctuations in the values determined in this study as with the increasing volume fraction, the load distribution inside the RVE changes due to changing packing factor, which is not considered in the modified rule of mixture for short fiber, where fibers are assumed straight. Longitudinal elastic modulus becomes around 12.5 times of that of pure polymer matrix at the volume fraction of 10%. Transverse elastic modulus becomes around 1.7 times of that of pure polymer matrix at the volume fraction of 10%.

The RVE is composed of polymer matrix of very low Young modulus reinforced by CNTs with very high Young modulus. With the increment of volume fraction, the CNTs contributes more to the strength of the composite, as a result overall strength of the composite increases with the
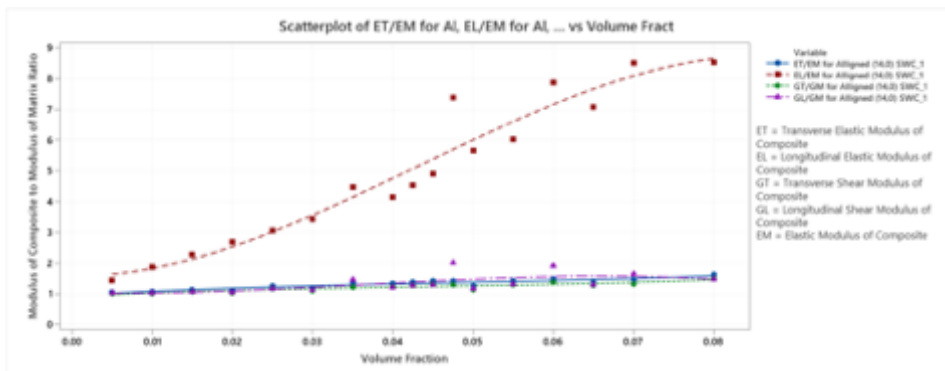
increment of volume fraction.

Transverse shear modulus of nanocomposite reinforced with aligned (8, 8) CNTs increases with the increasing volume fraction. After a volume fraction of 2.5%, it increases linearly. At a volume fraction of 10%, transverse shear modulus becomes around 1.55 times of that of pure polymer matrix.

Longitudinal shear modulus of nanocomposite reinforced with aligned (8, 8) CNTs increase with the increasing volume fraction with some fluctuating values.

Longitudinal shear modulus increases with a few fluctuating values. At 10% volume fraction, it becomes around 2.2 times of that of the pure polymer matrix.

3.8. Polymer composite reinforced with aligned (14, 0) CNT

For (14,0) aligned CNT, at waviness ratio = 0.012, wavelength ratio = 22.34, elastic modulus of CNT = 0.60 TPa: Volume fraction was varied from 0.5% to 10%. From the simulation software, the values of the constants in stiffness matrix have been determined.

Figure 13. Modulus Ratio vs Waviness Ratio for (14,0) SWCNT with Waviness ratio = 0.012 and wavelength ratio = 22.34

In Figure 13, variation of elastic modulus of nanocomposite reinforced with aligned (14, 0) CNTs with the increasing volume fraction has been illustrated. Both Longitudinal and Transverse Elastic modulus increases with increasing volume fraction.

Change of the longitudinal elastic modulus with increasing volume fraction found in the study have lower rate of increment than the values from modified rule of mixture. Longitudinal elastic modulus becomes around 8.5 times of that of pure polymer matrix at the volume fraction of 10%. Transverse elastic modulus becomes around 1.6 times of that of pure polymer matrix at the volume fraction of 10%.

Both transverse shear modulus and longitudinal Shear Modulus of nanocomposite reinforced with aligned (14, 0) CNTs increase with the increasing volume fraction. At a volume fraction of 10%, transverse shear modulus becomes around 1.5 times of that of pure polymer matrix. Longitudinal shear modulus increases with a few fluctuating values. At 10% volume fraction, it becomes around 1.5 times of that of the pure polymer matrix.

3.9. Nanocomposite reinforced with aligned (8,8) CNT and an interface material

To study the effect of an interface material between the CNT and the matrix, Epoxy with elastic modulus of 15 GPa and Poisson's ratio of 0.35 was used in the model. The volume fraction of CNT fiber was 2.5% and the interface thickness was 10% of the tube diameter. A wavelength ratio of 22.73 was considered. From the simulation software, the values of the constants in stiffness matrix have been determined.
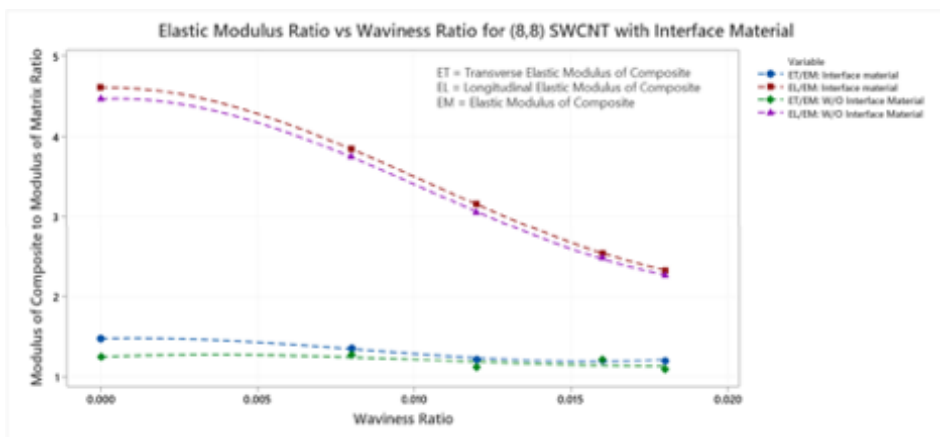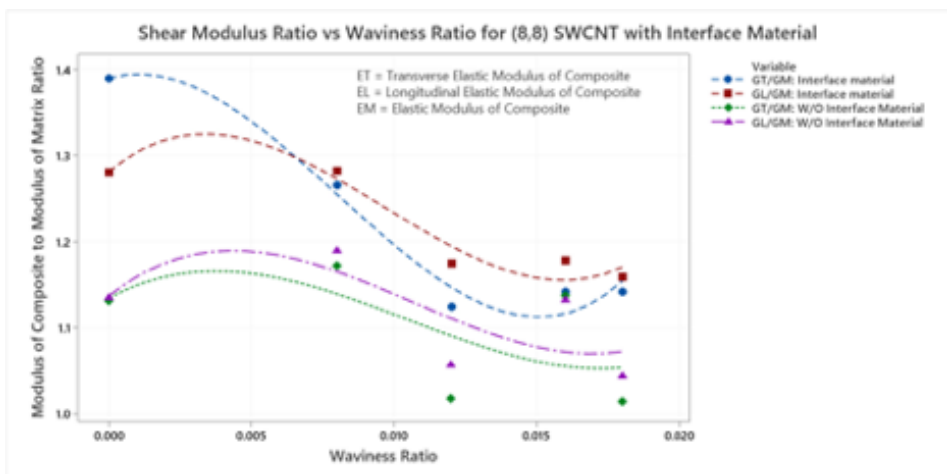

Figure 14. Elastic Modulus Ratio vs Waviness Ratio for (8,8) SWCNT reinforced nanocomposite with and without interface material of 10% thickness

In Figure 14, comparison of elastic modulus of nanocomposite reinforced with aligned (8, 8) CNTs with nanocomposites with an interface material have been illustrated. Longitudinal elastic modulus for a straight CNT with the interface material is around 3.6% higher than that of the straight CNT without interface material. For a waviness ratio up to 1.8%, longitudinal elastic modulus for nanocomposite with interface material decreases by 50%; where the value is 49% for the nanocomposite without interface material.

Transverse elastic modulus for a straight CNT with the interface material is around 18% higher than that of the straight CNT without interface material. For a waviness ratio up to 1.8%,

Transverse elastic modulus for CNT with interface material decreases by 18%; where the reduction is 12% for the CNT without interface material.

Figure 15. Shear Modulus Ratio vs Waviness Ratio for (8,8) SWCNT reinforced nanocomposite with and without interface material of 10% thickness

Transverse shear modulus and longitudinal shear modulus (Figure 15) of nanocomposite reinforced with aligned (8, 8) CNTs have been compared with composite with an interface material. With the increasing volume fraction both Transverse and Longitudinal, shear modulus decreases with less fluctuating values for composites with interface material.

Transverse shear modulus for a straight CNT with the interface material is around 22% higher than that of the straight CNT without interface material. For a waviness ratio up to 1.8%, transverse shear modulus for CNT with

interface material decreases by 18%; where the reduction is 10% for the CNT without interface material.

Longitudinal shear modulus for a straight CNT with the interface material is around 18% higher than that of the straight CNT without interface material. For a waviness ratio up to 1.8%, longitudinal shear modulus for CNT with interface material decreases by 10%; where the reduction is 8% for the CNT without interface material.

While studying the effect of interface material, the interactions like chemical reactions between the interface and matrix or interface and fiber were not considered. As the interface material added a layer of stronger material on the fiber inside the matrix, it is expected that it becomes stronger than the composite without interface material. Longitudinal shear modulus decreases with increasing waviness ratio in an irregular way and decreases by 22.4% as the waviness varies up to 3.2%.

In the case of (14, 0) CNT, the curves for transverse elastic modulus, longitudinal shear modulus and transverse shear modulus have less amount of fluctuation than that of the (8,8) CNT.

Interface material has a consistent effect on elastic modulus, whereas the change of shear modulus is inconsistent.

4. CONCLUSION

The strength and flexibility of carbon nanotubes makes them of potential use in controlling other Nano-scale structures, which suggests that they will have an important role in nanotechnology engineering. In a composite material the embedded CNTs are not straight rather wavy in nature. The literature review proves that there is interest in the effect of waviness on the bulk property of the composite. Nevertheless, in this study it was observed how the waviness affects the strength of CNT itself.

In this work, the change of mechanical properties in a single walled CNT with the increasing waviness has been studied. It is found that waviness significantly impacts the moduli of a CNT, resulting in almost 85% decrease for a waviness value of 3.2%. Using the derived values, polymer nanocomposite containing wavy Single-Walled Carbon Nanotubes (SWCNTs) has been characterized by utilizing a continuum approach. The CNTs used in the study was modeled as a curved solid beam in a representative volume element (RVE) of a polymer matrix. The study was carried out with randomly oriented CNTs that provided similar pattern of

curves for longitudinal and transverse directions. In addition, the effect of increasing volume fraction on strength of composite was compared with modified rule of mixture for short fiber, which validates the method of this study.

Effect of interface material between the polymer and the CNTs were studied to observe the reinforcement of strength of the nanocomposite.

It was observed that the Elastic modulus decreases with increasing waviness of CNT, but after a certain value of waviness ratio, the decreasing rate becomes insignificant. Additionally, the modulus of the CNT decreases with diameter, while having drastic change in the larger diameter region. The atomic bonds within the cusp zones could attribute to this phenomenon.

Though composite reinforced with CNTs follow similar trend with the atomic model, at higher waviness ratio, alignments of CNTs have less impact on the modulus of the composite.

Moreover, the overall strength of the composite increases non-linearly with the increment of volume fraction, and finally, interface material reinforces the mechanical properties of the composite. Interface material has a consistent effect on elastic modulus, whereas the change of shear modulus is inconsistent.

REFERENCES

[1]   Iijima, S., Helical microtubules of graphitic carbon. nature, 1991. 354(6348): p. 56- 58.

[2]   Che, J., T. Çağın, and W.A. Goddard Iii, Generalized extended empirical bond-order dependent force fields including nonbond interactions. Theoretical Chemistry Accounts, 1999. 102(1-6): p. 346-354.

[3]   Hernandez, E., et al., Elastic properties of C and B x C y N z composite nanotubes.Physical Review Letters, 1998. 80(20): p. 4502.

[4]   Sánchez-Portal, D., et al., Ab initio structural, elastic, and vibrational properties of carbon nanotubes. Physical Review B, 1999. 59(19): p. 12678.

[5]   Salvetat, J.-P., et al., Mechanical properties of carbon nanotubes. Applied Physics A, 1999. 69(3): p. 255-260.

[6]   Robertson, J., Realistic applications of CNTs. Materials Today, 2004. 7(10): p. 46-52.

[7]   Treacy, M., T. Ebbesen, and J. Gibson, Exceptionally high Young's modulus observed for individual carbon nanotubes. 1996.

[8]   Krishnan, A., et al., Young's modulus of single-walled nanotubes. Physical Review B, 1998. 58(20): p. 14013.

[9]   Wong, E.W., P.E. Sheehan, and C.M. Lieber, Nanobeam mechanics: elasticity, strength, and toughness of nanorods and nanotubes. Science, 1997. 277(5334): p. 1971-1975.

[10]   Poncharal, P., et al., Electrostatic deflections and electromechanical resonances of carbon nanotubes. science, 1999. 283(5407): p. 1513-1516.

w   Iijima, S., et al., Structural flexibility of carbon nanotubes. The Journal of chemical physics, 1996. 104(5): p. 2089-2092.

[12]   Gao, G., T. Cagin, and W.A. Goddard III, Energetics, structure, mechanical and vibrational properties of single-walled carbon nanotubes. Nanotechnology, 1998. 9(3): p. 184.

[13]   Xin, Z., Z. Jianjun, and O.-Y. Zhong-Can, Strain energy and Young's modulus of single-wall carbon nanotubes calculated from electronic energy-band theory. Physical Review B, 2000. 62(20): p. 13692.

[14]   Belytschko, T., et al., Atomistic simulations of nanotube fracture. Physical Review B, 2002. 65(23): p. 235430.

[15]   Zhang, P., et al., Fracture nucleation in single-wall carbon nano-tubes under tension: a continuum analysis incorporating interatomic potentials. Journal of Applied Mechanics, 2002. 69(4): p. 454-458.

[16]   Zhang, P., et al., The elastic modulus of single-wall carbon nano-tubes: a continuum analysis incorporating interatomic potentials. International Journal of Solids and Structures, 2002. 39(13): p. 3893-3906.

[17]   Jin, Y. and F. Yuan, Simulation of elastic properties of sin-gle-walled carbon nanotubes. Composites Science and Technology, 2003. 63(11): p. 1507-1515.

[18]   Li, C. and T.-W. Chou, A structural mechanics approach for the analysis of carbon nanotubes. International Journal of Solids and Struc-tures, 2003. 40(10): p. 2487-2499.

[19]   Li, C. and T.-W. Chou, Elastic moduli of multi-walled carbon nanotubes and the effect of van der Waals forces. Composites Science and Technology, 2003. 63(11): p. 1517-1524.

[20]   Fan, C., Y. Liu, and C. Hwu, Finite element simulation for es-timating the mechanical properties of multi-walled carbon nanotubes. Applied Physics A, 2009. 95(3): p. 819- 831.

[21]   Andrews, R., et al., Fabrication of carbon multiwall nanotube/ polymer composites by shear mixing. Macromolecular Materials and Engineering, 2002. 287(6): p. 395-403.

[22]   Qian, D., et al., Load transfer and deformation mechanisms in carbon nanotube- polystyrene composites. Applied physics letters, 2000. 76(20): p. 2868-2870.

[23]   Schadler, L., S. Giannaris, and P. Ajayan, Load transfer in carbon nanotube epoxy composites. Applied Physics Letters, 1998. 73(26): p. 3842-3844.

[24]   Sandler, J., et al., Development of a dispersion process for carbon nanotubes in an epoxy matrix and the resulting electrical properties. Polymer, 1999. 40(21): p. 5967- 5971.

[25]   Mahboob, M. and M. Zahabul Islam, Molecular dynamics simulations of defective CNT-polyethylene composite systems. Computational Materials Science, 2013. 79: p. 223-229.

[26]   Islam, M.Z., M. Mahboob, and R.L. Lowe, Mechanical properties of defective carbon nanotube/polyethylene nanocomposites: A molecular dynamics simulation study. Polymer Composites, 2014.

[27]   Shaffer, M.S. and A.H. Windle, Fabrication and characterization of carbon nanotube/poly (vinyl alcohol) composites. Advanced Materials, 1999. 11(11): p. 937- 941.

[28]   Fisher, F., R. Bradshaw, and L. Brinson, Effects of nanotube waviness on the modulus of nanotube-reinforced polymers. Applied Physics Letters, 2002. 80(24): p. 4647- 4649.

[29]   Fisher, F., R. Bradshaw, and L. Brinson, Fiber waviness in nanotube-reinforced polymer composites—I: Modulus predictions using effective nanotube properties. Composites Science and Technology, 2003. 63(11): p. 1689-1703.

[30]   Bradshaw, R., F. Fisher, and L. Brinson, Fiber waviness in nano-tube-reinforced polymer composites—II: modeling via numerical approximation of the dilute strain concentration tensor. Composites Science and Technology, 2003. 63(11): p. 1705- 1722.

[31]   Zak, G., et al., Mechanical properties of short-fibre layered composites: prediction and experiment. Rapid Prototyping Journal, 2000. 6(2): p. 107-118.

[32]   Tserpes, K. and P. Papanikos, Finite element modeling of single-walled carbon nanotubes. Composites Part B: Engineering, 2005. 36(5): p. 468-477.

[33]   Barbero, E.J., Finite Element Analysis of Composite Materials. 2007: CRC press.

[34]   Brcic, M., M. Canadija, and J. Brnic, Influence of Waviness and Vacancy Defects on Carbon Nanotubes Properties. Procedia Engineering, 2015. 100: p. 213-219.

[35]   Paunikar, Shweta & Kumar, Surendra. (2014). Effect of CNT waviness on the effective mechanical properties of long and short CNT reinforced composites. Computational Materials Science. 95. 21–28. 10.1016/j.commatsci.2014.06.034.